[American Journal of Science, Vol. 309, January, 2009, P. 43–84, DOI 10.2475/01.2009.02]

PETROLOGY OF AN INVERTED BARROVIAN SEQUENCE OF METAPELITES IN SIKKIM HIMALAYA, INDIA: CONSTRAINTS ON THE TECTONICS OF INVERSION

SOMNATH DASGUPTA*,†, SUMIT CHAKRABORTY** and SUDIPTA NEOGI***

ABSTRACT. The lesser Himalayan sequence in Sikkim exposes an unusually complete inverted Barrovian sequence of metapelitic rocks. A number of different bulk compositions are interlayered along the prograde sequence, providing an excellent natural laboratory for studying the controls of pressure, temperature and composition on stability of mineral assemblages. Using three different approaches for determining pressures and temperatures, and making use of the bulk chemical constraints, we show that all three methods yield consistent estimates of pressures and temperatures once the strengths and weaknesses inherent to each approach are critically evaluated. The metamorphic field gradient along two separate traverses are found to be positive (60 °C/kbar in east Sikkim and 70 °C/kbar in north Sikkim) - pressure *as well as* temperature increases continually up to the highest grade. The various bulk compositions allow different assemblages to be used to establish the coherence of the sequence. In combination these place tight constraints on the permissible tectonic mechanisms for the production of this inverted metamorphic sequence. Neither older hot iron type models, nor more recent models that invoke thrusting (post- or syn-metamorphic) as a mechanism of inversion can produce such a coherent package inverted in pressure as well as temperature. On the other hand, the observations are more consistent with the predictions of channel flow type tectonics. In particular, a recent geodynamic model of subduction-collision that takes into account high heat generation (as found in these Himalayan metapelites) and incorporates the effects of the resulting melting (reduction of viscosity and enhancement of buoyancy) on the tectonic evolution, predicts such inversion of coherent blocks as an unavoidable consequence. Such melting triggered inversion and exhumation as a coherent, fault bounded block explains many features of the inverted sequence in Sikkim and it is not necessary to invoke inversion by multiple thrusting events.

INTRODUCTION

One of the best developed Barrovian sequences in metapelitic rocks occurs over the entire length of the Himalayan mountain chain. The sequence is inverted so that progressively higher grade rocks occur at higher structural levels. This inverted metamorphic sequence (IMS) in turn is spatially closely related to the Main Central Thrust Zone (MCTZ) that juxtaposes rocks of the Lesser Himalaya with those of the Higher Himalaya. Much of the literature on metamorphism and origin of the IMS has focussed on thermobarometry because of the obvious significance of these data for tectonic models of development of the MCTZ and the evolution of the Himalayan range as a whole (see Pecher, 1989; Guillot, 1999; as well as reviews in Macfarlane and others, 1999; Hodges, 2000; Jain and others, 2002 for an overview; more recent contributions include Fraser and others, 2000; Stephenson and others, 2000; Beyssac and others, 2004). Quite aside from this tectonic significance, the wide extent and continuous nature of the Barrovian sequence provides an excellent natural laboratory to study various petrological processes such as bulk compositional control on the

*Indian Institute of Science Education and Research; HC-VII, Sector III, Salt Lake, Kolkata-700 106, India

**Institut für Geologie, Mineralogie und Geophysik, Ruhr Universität Bochum, D - 44780 Bochum, Germany

***Geological Survey of India, Central Headquarters, 27, Jawaharlal Nehru Road, Kolkata - 700 016, India

†Corresponding author: Sumit.Chakraborty@rub.de

appearance of key phases and the mobility of elements during metamorphism. The known tectonic boundary conditions and the lack of overprinting by subsequent orogenic processes make these rocks particularly attractive. The eastern Himalayan Sikkim - Darjeeling region exposes a very complete sequence of metapelites and is one of the first regions that introduced the concept of an IMS (Mallet, 1874; Bose, 1891; Ray, 1947, 1949). More recent contributions on various aspects of rocks from Sikkim (Lesser as well as Higher Himalaya) include Mohan and others (1989), Neogi and others (1998), Ganguly and others (2000), Chakraborty and others (2003), Dasgupta and others (2004), Catlos and others (2004), Harris and others (2004), Dubey and others (2005), and Searle and Szulc (2005). We have carried out a geochemical–petrological study of rocks from two traverses in this region with emphasis on evaluating the bulk compositional as well as thermobaric control on the development of the different assemblages. The added information on bulk composition control allows us to:

(i) Depict how the sequence of phase assemblages that are stable in a rock volume moving along a given P-T path differ for different bulk compositions. The variations we consider correspond to real, measured bulk composition variations encountered on an outcrop scale rather than idealized endmember compositions.

(ii) Carry out thermobarometry using different approaches and combine our results with earlier P-T estimates to discuss the strengths and weaknesses of the different approaches. This results in better constrained P-T conditions of equilibration as well as metamorphic field gradients.

(iii) Evaluate the nature and extent of element mobility during metamorphism in this Barrovian sequence, and (iv) combine the results of thermobarometry with those from a recent geodynamic modeling (Faccenda and others, 2008) to suggest a mechanism for production of the inverted metamorphic sequence in this area consistent with the petrological observations.

GEOLOGICAL SETTING AND STRUCTURAL CONVENTION

Figure 1 shows a simplified map of the main geological units in the Himalaya (fig. 1A), a regional geological map of the area around the two traverses (fig. 1B), and cross sections showing the location of the samples in relation to the topography (figs. 1C and D). The Sikkim Himalaya has been classically subdivided into a series of geotectonic domains with distinct geological attributes and histories (for example see Sinha Roy, 1982). Beginning from the south, the Sub Himalayan domain comprises the unmetamorphosed to weakly metamorphosed mollase type deposits of the Siwaliks (Mio-Pliocene), followed northward successively by a thin strip of Gondwana sediments (Carboniferous-Permian), carbonates (Buxa Formation) and a thick metasedimentary sequence of dominantly pelites with subordinate psammite, calcareous and metabasic rocks (Daling Group), constituting the Lesser Himalayan Belt. The Main Boundary Thrust (MBT) separates the Siwaliks of the Sub-Himalaya from the overlying rocks of the Lesser Himalayan Belt. The lesser Himalayan rocks are followed by the Higher Himalayan Belt of medium to high grade crystallines, the Higher Himalayan Crystallines (HHC), again made up dominantly of pelitic rocks (pelitic gneisses and migmatites) with interbedded quartzites, calc-silicate rocks, metabasites and small bodies of granites. The boundary between the lesser and higher Himalaya is marked by the Main Central Thrust (MCT) or an extended zone of ductile deformation, the Main Central Thrust Zone (MCTZ) (for example see Pecher, 1989 and Stephenson and others, 2000 for discussions). In the far north, a thick pile of fossiliferous Cambrian to Eocene sediments belonging to the Tethyan Belt (Tethyan Sedimentary Zone) overlie the HHC on the hanging wall side of a series of north-dipping normal faults constituting the South Tibetan Detachment System (STDS). A well-foliated, highly mylonitized intrusive granite gneiss unit (Lingtse Gneiss, fig. 1B) crops out within the lesser

Himalayan rocks. The lesser Himalayan metapelitic rocks of the Daling group are the topic of this study.

In keeping with much of the Himalayan literature, we describe the planar structures in our study area using the following convention: the primary compositional banding, where preserved in lower grades, is termed S_0. A relic early foliation that is defined only by inclusions in porphyroblasts and is discordant to the main matrix foliation, preserved primarily in the lower grade rocks, is termed S_1. The main matrix foliation defined by phyllosilicates is termed S_2; crenulations of this structure, when accompanied by development of new foliation defining minerals, is described as S_3. Metamorphic isograds are by and large parallel to S_2. Finally, all of these structures are folded, along with isograds, in the mesoscopic map pattern of Sikkim so that metamorphic grade increases eastward, northward and westward from what is known as the culmination of the Tista dome. The axial plane of this structure is termed S_4. We emphasize that this nomenclature is purely descriptive for different groups of planar structures without any connotation about the number of deformation events.

PETROGRAPHY, BULK AND MINERAL CHEMISTRY, AND INFERRED REACTIONS

Sample Location

We have studied metapelites exposed along two transects in East and North Sikkim (GPS locations of the samples used in this study are given in table 1 and are also available electronically in Supplemental table 1, http://earth.geology.yale.edu/~ajs/SupplementaryData/2008/08DasguptaTable1.pdf). The line of the transects in figure 1B, 22 km for the eastern and 38 km for the northern sectors, are shorter than the actual traverses in the field that follow roadcuts and river valleys. The rocks show variations in mineral assemblages on all scales ranging from thin sections to outcrop (meter-scale) and regional (kilometer scale). The first two are shown to be related to variations in bulk composition while the latter is related to differences in peak pressures and temperatures of metamorphism as well as composition. Interbands of quartzite and lenses of metabasites are present locally throughout the exposed metapelitic sequence. Quartz veins are present at all grades and their abundance increases with metamorphic grade in general. Up to the staurolite grade the veins are of almost pure quartz, in the kyanite grade they contain quartz + plagioclase and at still higher grades they contain K-feldspar in addition. We have tried in all cases to obtain samples from fresh roadcuts that were as free of alteration and veins as possible.

Analytical Methods and Data Reduction

Bulk chemical analysis for major, minor and trace elements was carried out by Xray fluorescence spectroscopy (XRF) at the Ruhr Universität Bochum on a Phillips PW2404 instrument. Several thin sections were prepared from each sample and after petrographic observation, 48 samples from chlorite-biotite zone to sillimanite-muscovite zone along the two transects were selected for chemical analysis. The sample size for preparation of powders was 20 cm $\times$ 20 cm $\times$ 10 cm. Two aliquots of the powders were used $-$ 0.7 gm to prepare a molten glass tablet and 8 gm to prepare a pellet, respectively. Major elements were determined from the melt tablets (Si, Ti, Al, Mg, Fe, Ca, Mn, Na, K and P) whereas the powdered pellets were used for trace element determinations.

Four samples were analyzed 2 times each after a gap of 9 months to check long term reproducibility. Two samples were analyzed twice, one from a larger size specimen (30 cm $\times$ 30 cm $\times$ 10 cm), and the other from the regular size to check the effect of size on chemical data. For major elements, differences were less than 0.1 percent. Selected samples were also analyzed by instrumental neutron activation analysis (INAA) at the Universität zu Köln and confirmed the results presented here.

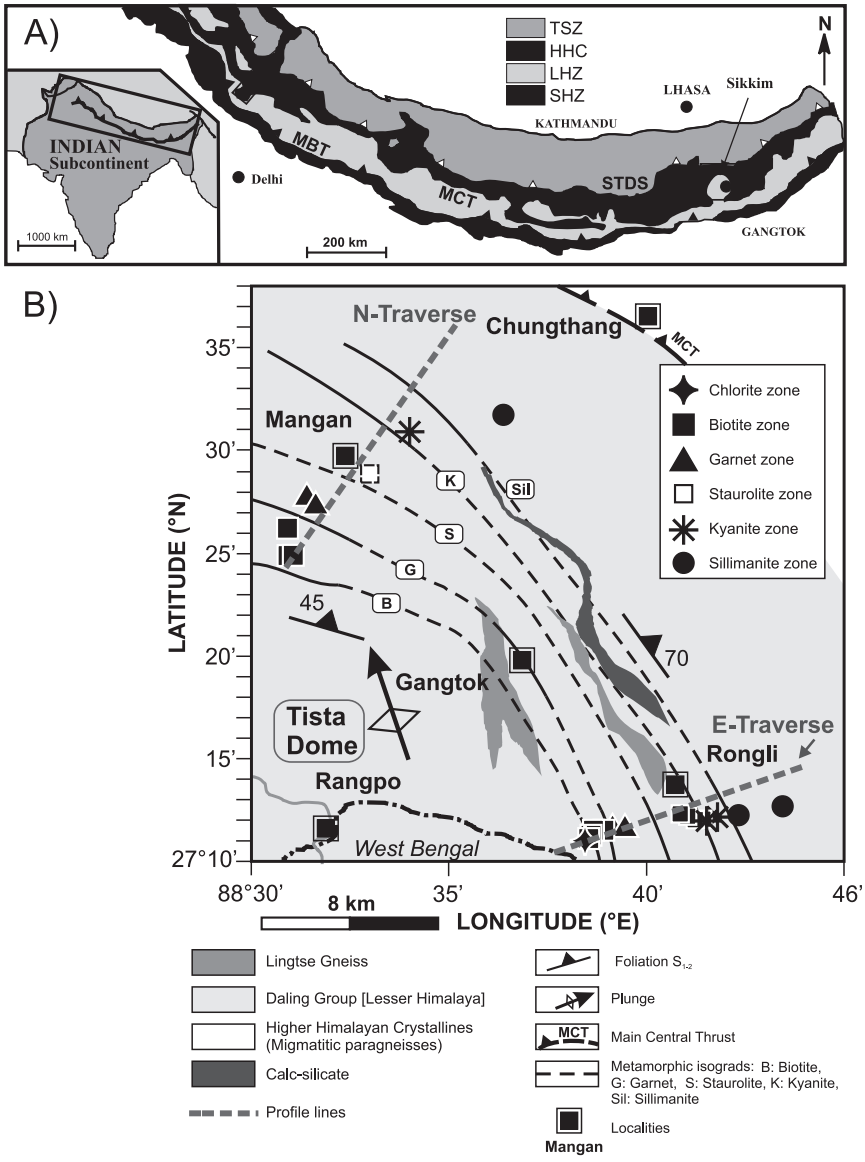

Fig. 1. (A) Generalized geological map of the Himalaya showing the main tectonic units and their bounding faults. TSZ: Tethyan Sedimentary Zone, HHC: Higher Himalayan Crystallines, LHZ: Lesser Himalayan Zone, SHZ: Sub-Himalayan Zone. MBT: Main Boundary Thrust, MCT: Main Central Thrust, STDS: South Tibetan Detachment System.

The study area in Sikkim is shown to the east. (B) Part of the lesser Himalayan section of Sikkim showing the sample locations and the disposition of the isograds. The profile directions for figures (C) and (D) are shown as straight dashed lines. GPS locations of samples are provided in table 1.

Aliquots of the same powders were used for the determination of the water contents by coulometric Karl-Fischer titration, CO_2 contents by IR spectroscopy and the Fe^{2+}/Fe^{3+} ratios by potentiometric titration, all at the Ruhr Universität Bochum.

Mineral compositions were determined primarily with a CAMECA SX 50 EPMA at Ruhr Universität, Bochum while some analyses were obtained using a CAMECA SX 51

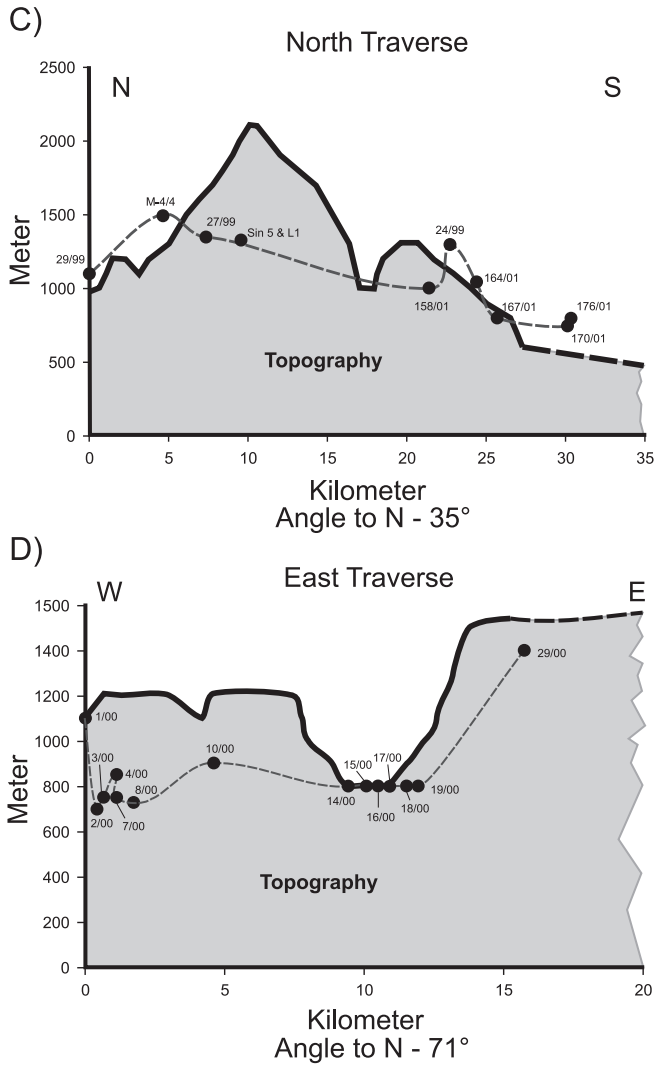

Fig. 1 (continued). (C) Sample locations projected onto the line of the north traverse of figure 1B. y axis = elevation, x-axis = distance along the traverse.

(D) Sample locations projected onto the line of the east traverse of figure 1B. y axis = elevation, x-axis = distance along the traverse.

Sample **129/87, 127/88** - north Sikkim, staurolite zone, next to Mangan

Sample **SIN8-** north Sikkim, kyanite zone, 3 km north of Mangan

Sample **15/95** - Same as location as L1.

Sample **187/xx** - north Sikkim, south of 170/xx and 176/xx (near the the town of Singtam, not shown in the map). "xx" is a wildcard for digits, such as 01, 02 which refer to the first, second *etc.* samples from the same outcrop.

Sample **13/95** and **36/93** - 2 km and 7 km north of 29/99, respectively, but not plotted since altitude is not known.

Please note that the locations of the following samples referred to in the text/tables could not be plotted distinctly due to lack of resolution on this scale:

Sample **143/01** - east Sikkim, Sill-Kfs zone, close to location 29/00;

Sample **20/00**, **25/00/CH**, **M-1/2** - All from near the town of Rongli.

Samples **135/01** - east Sikkim, indistinguishable from the location marked 7/00;

Sample **11/00** - east Sikkim, indistinguishable from the location marked 10/00;

Sample **31/95** - Located between 10/00 and 14/00 in east Sikkim, exact altitude unknown;

Sample **1C/00/3** and other similarly named samples - east Sikkim, same outcrop as that marked 1/00 (biotite grade);

Sample **36/00** - Slightly west of the location of 1/00.

TABLE 1

Compositional groups, typical sample numbers and location with their bulk compositional and mineralogical characteristics at different metamorphic grades

Metamorphic Grade and Bulk Chemical Characteristics	Compositional Group	Sample #s, N/E Traverse	GPS coordinates	Mineral Assemblages and Modal Abundance
Chlorite Group I: Al_2O_3 ~25 wt.%	**Normal**	#1/00/CH, E,	27°11.268, /88°38.581	Ms-Chl-Qtz-Ilm-Mag-Gr ± Kfs ± Pl Mode: (Qtz 35-42%, Ms 30 - 33%, Chl 25 - 30%, Pl 5-7%).
Group II: Al_2O_3 ~20 wt.% Rocks richer in Al_2O_3 are relatively less ferruginous (see fig 3).	**Normal**	#187/01, #187/03, #1870/3/CH, N,	GPS not known	Ms-Chl-Qtz-Ilm-Mag-Gr ± Kfs ± Pl Mode: (Qtz 35-42%, Ms 30 - 33%, Chl 25 - 30%, Pl 5-7%).
Biotite Group I a: Al_2O_3 ~ 18-24 wt% Fe_2O_3 ~ 4.5-5 wt%	**Normal**	#ID/00,E, #2/00/R/CH, E, #176/01,N, #170/01,N,	27°11.268, /88°38.581 27°11.465, /88°38.650 27°24.809, /88°30.935 27°24.809, /88°30.925	Ms-Chl-Qtz-Bt - Pl ± Ilm ± Tur ± Gr Mode: (Qtz 35-42%, Ms 30 - 33%, Bt 15 - 18%, Chl 10 - 12%, Pl 5-7%).
Group I b: Al_2O_3 ~ 14.5-17 wt% Fe_2O_3 ~ 6-8 wt%	**Normal**	#3/00/2, E, #4/00, E, #167/01, N,	27°11.465, /88°38.692 27°11.484, /88°38.858 27°26.092, /88°30.888	Ms-Chl-Qtz-Bt - Pl ± Ilm ± Tur ± Gr Mode: (Qtz 35-42%, Ms 30 - 33%, Bt 15 - 18%, Chl 10 - 12%, Pl 5-7%).
Group II: MgO ~ 5 wt%.	**Magnesian** ***(Normal - Bt)***	#1/00/A, E,	27°11.268, /88°38.581	Chl - Qtz -Pl ± Ms
Group III: MnO ~ 0.4 wt%, ~ 10 x other bulk compositions	**Mn-rich** ***(Normal + Grt)***	# 1C/00/3, E	27°11.288, /88°38.619	Ms - Chl - Qtz - Pl - Grt - Mag - Ilm - Gr.
Garnet Group I: low Al_2O_3; some Mn rich and Mg rich bulk compositions found	**Normal**	#8/00/CH, E, #158/01/CH, N,	27°11.616, /88°39.131; 27°27.711, /88°31.400	Ms - Qtz - Chl - Bt ± Pl - Ilm ± Grt ± Gr Mode: (Qtz 26-30%, Ms 35-40%, Bt 8-15%, Chl 8%, Grt 1-3%, Pl 5-8%)

TABLE 1
(continued)

Metamorphic Grade and Bulk Chemical Characteristics	Compositional Group	Sample #s, N/E Traverse	GPS coordinates	Mineral Assemblages and Modal Abundance
Garnet Group II: high Al_2O_3; some Mn rich and Mg rich bulk compositions found	**Aluminous, high Fe**	#24/99/1-1, N,	27°27.292′, /88°31.63	Ms - Qtz - Chl - Bt ± Pl - Ilm ± Grt ± Gr Mode: (Qtz 26-30%, Ms 35-40%, Bt 8-15%, Chl 8%, Grt 1-3%, Pl 5-8%)
Group III: Similar in Mn and even lower in Al content to garnet bearing rocks from the same outcrop (e.g. #8/00).	**Ferruginous** ***(Normal + Cld)***	#7/00/R4/CH & #7/00/R6/CH, E, #135/01, E	27°11.616, /88°39.131 GPS not known	Ms - Cld - Qtz - Chl - Bt - Ilm ± Gr ± Grt Mode: (Qtz 35-40%, Cld 12 - 16%, Grt 4-8%, Chl 8 - 16%, Ms 20 - 22%, Bt 8-10%, Pl 6-10%).
Group IV: Similar in Mn and even lower in Al content to garnet bearing rocks from the same outcrop (e.g. #8/00).	**Low Potassic (semi - pelite)** ***(Normal – Ms) Deduced on the basis of mineralogy***	#10/00, E,	27°11.628, /88°39.459;	Chl - Qtz - Grt - Pl - Bt - Ap - Ilm
Staurolite Group I: Equivalent of low alumina pelites from lower grades.	**Normal**	#17/00, E,	27°12.064, /88°41.397	Ms - Qtz -St - Pl - Bt - Ilm - Grt Mode: (Qtz 35 - 44%, Ms 15 - 17%, Bt 18 -22%, St 9 - 11%, Grt 5-10%, Pl 5 - 10%).
Group II: Deduced to be more aluminous on the basis of mineralogy	**Aluminous** ***(Normal + Ky)***	#11/00, E,	GPS not available	Ms -Bt -Grt -St - Ky - fibrolite -Grt - Ilm – Qtz ± Cld, secondary Chl.
Group III: CaO > 3.5 wt% compared to general range of 0.15 - 0.55 %.	**Calcic** *(Normal - St)*	#14/00/CH, E,	27°12.174, /88°41.026	Ms - Bt - Qtz - Pl - Grt - Ilm
Group IV: Low Mn bulk composition MnO < 0.05 wt%	**Mn - poor** *(Normal, with Mn poor Grt)*	#15/00/CH, E, #16/00/CH, E,	27°12.157, /88°41.137 27°12.100, /88°41.250	Ms - Qtz -St - Pl - Bt - Ilm - Grt
Group V: Deduced on the basis of mineralogy	**Fe-rich ?** *(Normal - Grt)*	#129/87,N,	GPS not available	Ms - Qtz - St -Pl - Bt - Ilm.

TABLE 1
(continued)

Metamorphic Grade and Bulk Chemical Characteristics	Compositional Group	Sample #s, N/E Traverse	GPS coordinates	Mineral Assemblages and Modal Abundance
Kyanite Group I: Equivalent of low alumina pelites from lower grades. (#Sin8 contains high CaO (1.2 - 1.4 wt%).	**Normal**	#19/00/02, E & #19/00/1/CH,E #Sin8,N, #27/99/1,N, #27/99/3,N,	27°12.135, /88°41.778 GPS not available 27°30.906, /88°33.981 27°30.906, /88°33.981	Grt - Bt - Pl - Qtz - Ms ± St (only as included phase) - Ky - Ilm. Mode: (Qtz 42-45%, Ms 15-17%, Bt 12 - 20%, Ky 4-8%, Grt 4-8%, Pl 10 - 15%).
Group II: Al_2O_3 >20 wt% High CaO (1.2 - 1.4 wt%)	**Aluminous** *(Normal - Grt)*	#19/00/1, E,	27°11.955, /88° 41.514	Qtz - Ms - Bt - Pl - Ky - Ilm
Group III: MnO highly enriched, up to 1 wt%.	**Mn - rich**	#18/00/CH, E, #18/00/2, E,	27°11.955, /88° 41.514 27°11.955, /88° 41.514	Qtz - Pl - Ms -Bt - Grt - Ilm ± Ky ± St.
Sillimanite – muscovite Both low Al, high Fe and high Fe, low Al groups represented.	**No bulk composition groups defined**	#20/00, E, #29/99/CH & #M4/1, N,	27°12.195, /88°42.29; 27°31.757, /88°36.369	Qtz -Bt - Ms - Sil ± Grt - Pl ± Ky - Ilm
Sillimanite - K-Feldspar Both low Al, high Fe and high Fe, low Al groups represented.	**No bulk composition groups defined**	#29/00, E,	27°12.695, /88°43.436	Qtz - Bt - Kfs -Pl - Sil ± Grt - Ilm.

EPMA at the Geological Survey of India Laboratory at Faridabad, a CAMECA SX 50 EPMA at the University of Arizona, USA, and with a JEOL JXA-8600 EPMA at Jadavpur University, Kolkata. Operating conditions were 15 kV acceleration potential, 15 nA probe current and 2 to 5 μm beam diameter. Natural and synthetic mineral standards were used for the analyses. An on-line ZAF/PAP correction procedure was used to correct for absorption, fluorescence and atomic number.

Identification of accessory phases was verified using EDX on the EPMA or on a SEM at the Ruhr Universität Bochum.

The mineral compositions obtained from the electron microprobe for key minerals were reduced using the following schemes. For garnet, the analyses were normalized to 24 oxygens and the octahedral position was filled with Fe^{3+} if necessary. The remaining Fe was assigned as Fe^{2+} to calculate mole fractions of almandine, pyrope, spessartine and grossular. Plagioclase analyses were normalized to 8 oxygens and the resulting atom proportions were used to calculate albite, anorthite and orthoclase proportions. Biotite analyses were normalized to 22 oxygens, without any correction for Fe^{3+}. Due to the high Fe content in our white micas, it was not convenient to use the scheme of Holdaway and others (1988). Instead we have reduced the chemical data to muscovite $KAl_3Si_3O_{10}(OH)_2$, paragonite $NaAl_3Si_3O_{10}(OH)_2$, celadonite $KMgAlSi_4O_{10}(OH)_2$, Fe-celadonite $KFeAlSi_4O_{10}(OH)_2$ and pyrophyllite $Al_2Si_4O_{10}(OH)_2$ components. These are the end members used in the Holland and Powell (1998) thermodynamic database and is therefore convenient for further calculations.

Modal abundances were calculated from mass balance relations between bulk and mineral chemical analyses.

Compositional and Petrographic Characteristics of the Sequence

Bulk chemical compositions of all samples are provided in Supplemental table 2 (http://earth.geology.yale.edu/~ajs/SupplementaryData/2008/09DasguptaTable2.doc) and representative mineral compositions in Supplemental table 3 (http://earth.geology.yale.edu/~ajs/SupplementaryData/2008/10DasguptaTable3A.doc; http://earth.geology.yale.edu/~ajs/SupplementaryData/2008/11DasguptaTable3B.doc; http://earth.geology.yale.edu/~ajs/SupplementaryData/2008/12DasguptaTable3C.doc; http://earth.geology.yale.edu/~ajs/SupplementaryData/2008/13DasguptaTable3D.doc; http://earth.geology.yale.edu/~ajs/SupplementaryData/2008/14DasguptaTable3E.doc; http://earth.geology.yale.edu/~ajs/SupplementaryData/2008/15DasguptaTable3F.doc; http://earth.geology.yale.edu/~ajs/SupplementaryData/2008/16DasguptaTable3G.doc).

Sample locations along with classification into chemical subgroups and mineral assemblages, modal abundances, mineral chemistry and textural attributes of each group have been summarized in table 1, with more details available electronically in an extended version (Supplemental table 1, http://earth.geology.yale.edu/~ajs/SupplementaryData/2008/08DasguptaTable1.pdf).

Considering the whole-rock chemical analyses in conjunction with (a) plotting positions on AFM diagrams (fig. 2) and (b) variation of mineral assemblages in samples collected from the same outcrops, several compositional groups were identified (table 1). At each metamorphic grade, there is a suite of high Al, low Fe and a suite of low Al, high Fe pelites, typically with different mineral assemblages. The low Al pelites have been designated as "normal" pelites in this work and all other compositional groups are with reference to this in terms of composition as well as mineral assemblage. For example, *Mn-rich* and *(Normal + garnet)* imply a bulk rock composition richer in Mn relative to the normal composition and that the mineral assemblage in this rock contains garnet in addition to all phases present in the normal bulk composition. In addition to the subdivisions based on Al content noted above, other compositional groups found are: biotite grade, magnesian and Mn-rich; garnet grade, ferruginous and K-poor semi-pelites; staurolite grade, aluminous, calcic, Mn-poor and

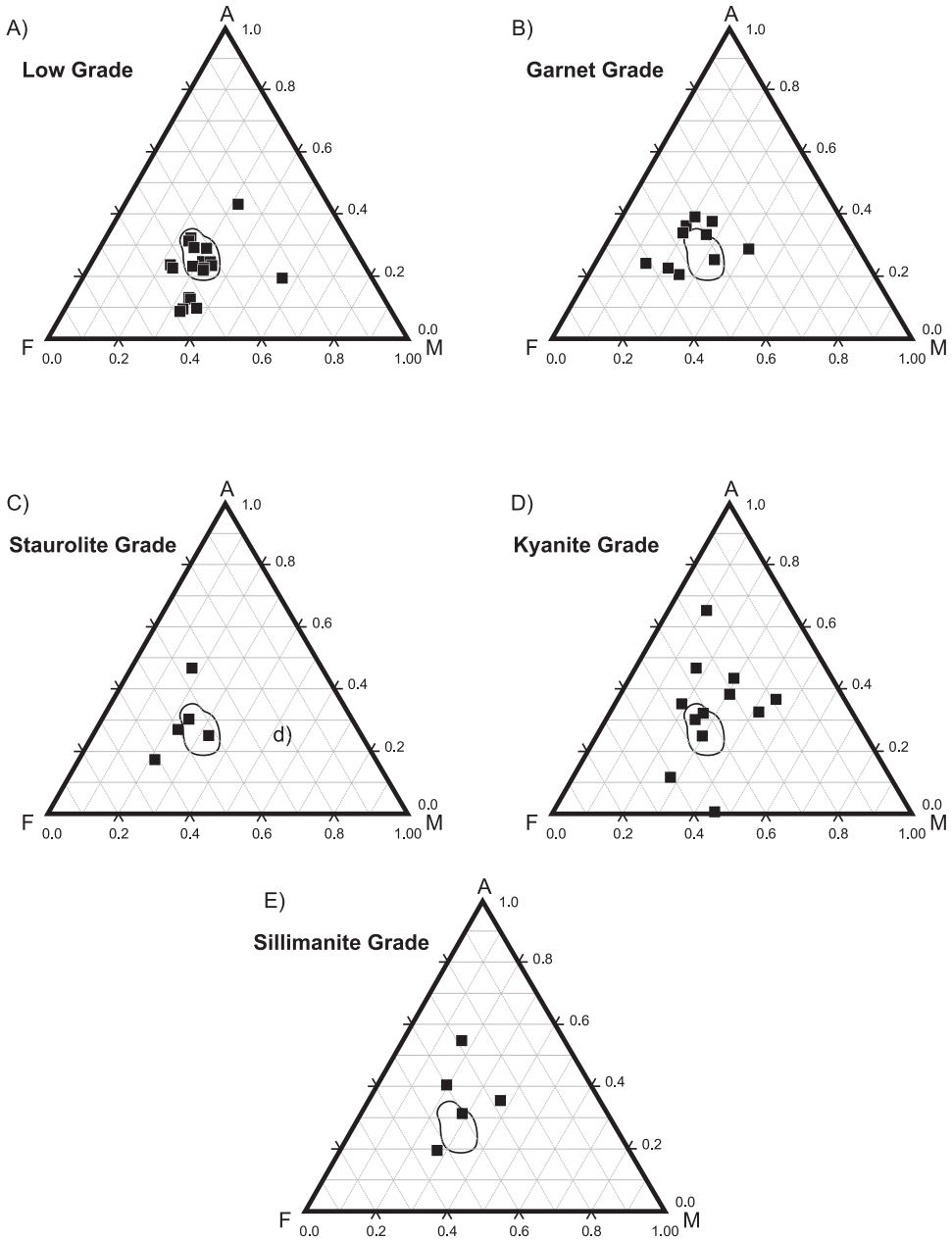

Fig. 2. AFM diagrams showing bulk chemical composition of metapelites as a function of metamorphic grade. The circled field in each triangular plot represents the compositional field of 'normal' (see text) metapelites in the low grade (chlorite-biotite grade) samples. (A) Chlorite-biotite grade samples, (B) garnet grade, (C) staurolite grade, (D) kyanite grade, (E) sillimanite grade. Grades are defined with respect to appearance of index minerals in 'normal' metapelites. See text for details.

Fe-rich; and kyanite grade, aluminous and Mn-rich. At the higher sillimanite-muscovite and sillimanite - K-feldspar grades the compositions become more of a continuum and in the absence of distinct phase assemblages, it is not meaningful to define subgroups. Only reactions and changes in phase assemblages in the normal bulk composition were

used to define the location of isograd boundaries. References to metamorphic zones and grades in the text are understood in this sense. As will be clear from the data in table 1 (see also Supplemental tables 1 and 2; http://earth.geology.yale.edu/~ajs/SupplementaryData/2008/08DasguptaTable1.pdf http://earth.geology.yale.edu/~ajs/SupplementaryData/2008/09DasguptaTable2.doc), not imposing this constraint would result in a haphazard sequence of appearance and disappearance of key metamorphic minerals (garnet, for example) along a traverse that runs across a series of isograd boundaries marking continuously increasing metamorphic grades. Some appearances/disappearances of minerals controlled by variations in bulk composition found in the region are as follows (all detailed in Supplemental table 1, http://earth.geology.yale.edu/~ajs/SupplementaryData/2008/08DasguptaTable1.pdf):

In the biotite zone, increasing Mg suppresses biotite formation in favor of chlorite, and increasing Mn favors the appearance of garnet. In the garnet zone, increasing Fe, even at the expense of Al, promotes formation of chloritoid rather than garnet. With decreasing K at the same grade muscovite disappears. In the staurolite zone, increasing Al promotes formation of kyanite, increasing Ca (even with increased Fe and Zn) suppresses the formation of staurolite and increase in Fe can cause the disappearance of garnet. In the kyanite zone, garnet is absent if the composition is more aluminous than normal.

The effects of these compositional distinctions (table 1 and Supplemental table 1, http://earth.geology.yale.edu/~ajs/SupplementaryData/2008/08DasguptaTable1.pdf) make it impossible to map isograds based on field observations alone. However, when drawn in consideration of chemical analyses, the isograds define a very regular pattern (for example fig. 1B) and the different bulk compositions help to constrain the P-T conditions of equilibration better by providing additional constraints.

Mineral assemblages are listed in table 1 and an extended version of the table, available electronically as Supplemental table 1, http://earth.geology.yale.edu/~ajs/SupplementaryData/2008/08DasguptaTable1.pdf provides a complete summary of the main petrographic and mineral chemical features of the samples. Some typical samples are illustrated in figure 3 and the variation of modal abundances as a function of metamorphic grade is illustrated in figure 4. In general, grain size increases with metamorphic grades and mineral compositions show systematic variations with changing bulk composition within a grade as well as across isograd boundaries in a given bulk composition.

Garnets span a wide range of composition and show a variety of compositional zoning patterns (Supplemental table 1, http://earth.geology.yale.edu/~ajs/SupplementaryData/2008/08DasguptaTable1.pdf, fig. 5). Garnets show normal growth zoning with Mn-rich cores at lower grades in normal pelites (fig. 5A). With increasing grades, the extent of growth zoning diminishes (for example staurolite grade, diffusive homogenization?), Mn-rich rims appear in some garnets (fig. 5B) and at the very highest grades (sillimanite and higher) diffusion zoning of Fe and Mg are formed at the rims during cooling. There are additional complications in some cases, such as growth zoning following inclusion trails (for example fig. 5C, sillimanite grade) and coalescence of multiple nuclei (fig. 5D, sillimanite - K-feldspar grade). Within the same zone and in adjacent outcrops, different bulk compositions can result in different kinds and extents of zoning in garnet (for example aluminous vs. normal pelites in staurolite zone, Supplemental table 1, http://earth.geology.yale.edu/~ajs/SupplementaryData/2008/08DasguptaTable1.pdf). These complications must be considered in choosing points for microprobe analyses for thermobarometry.

Plagioclase compositions vary from X_{An} = 0.03 to 0.43 from the lowest to the highest grades. In a given bulk composition, X_{An} increases with metamorphic grade. We found zoned plagioclase only at low (chlorite - biotite) grades. Plagioclase

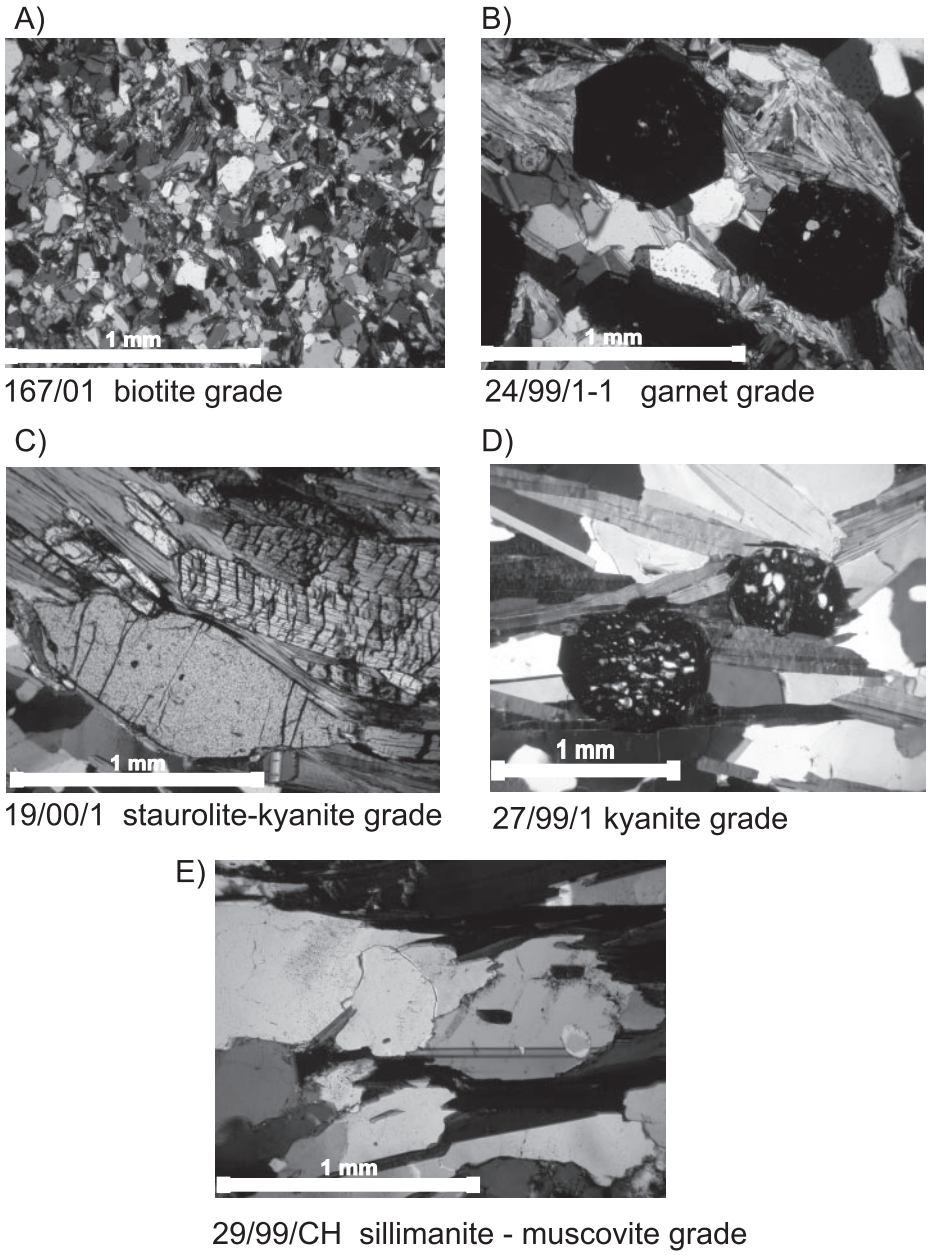

Fig. 3. Microphotographs of samples along a section across the Barrovian sequence. Crossed polarized light. Scale bars are 1 mm in each case. Note the lack of pervasive deformation at all grades, as well as the general trend of increase in grain size with grade. The sample number and the grade are noted below each panel. (A) quartz - plagioclase - biotite assemblage of a biotite zone sample. Note the lack of flattening of quartz and almost equilibrated foam texture, (B) garnet porphyroblasts from a garnet zone sample, (C) staurolite and kyanite coexisting in a sample from a location marking the first appearance of kyanite, (D) garnet porphyroblasts in a rock from the kyanite zone. Note the undeformed quartz grains, and (E) first appearance of melt in the sillimanite - muscovite zone.

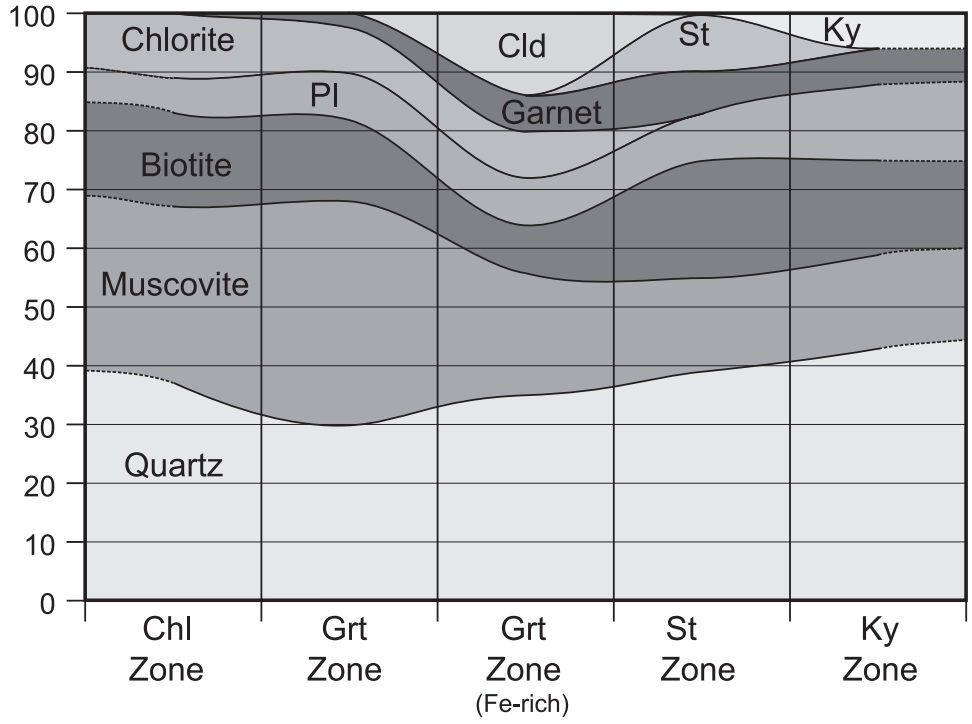

Fig. 4. Variation in modal abundance of minerals as a function of metamorphic grade. Note that for garnet grade, the modal abundances in normal as well as Fe-rich metapelites are shown, to show chloritoid abundance for comparison.

composition varies with distance from garnet in a thin section only in garnet grade rocks. At any given grade, there is a large difference in composition of plagioclase between garnet-bearing and garnet-free samples.

White mica is conspicuously enriched in the celadonite and Fe-celadonite components. Paragonite content of the mica increases with metamorphic grade up to the staurolite zone, as expected due to progressive closure of the solvus with temperature. However, at the kyanite grade, with the first appearance of leucosomes, there is a sharp drop of the paragonite content (Supplemental table 1, http://earth.geology.yale.edu/~ajs/SupplementaryData/2008/08DasguptaTable1.pdf).

Biotite composition shows restricted variability across the grades (X_{Fe} = 0.5–0.68). Within this range, however, X_{Fe} in biotite depends on bulk composition as well as metamorphic grade and is therefore difficult to systematize. At the sillimanite - K-feldspar isograd, there is an abrupt increase in Ti content of biotite, with ilmenite present both below and above the isograd boundary.

Model mineral reactions inferred for the sequence from textural and chemical criteria are summarized in table 2.

Quantifying pressure, temperature and activity of water during metamorphism

Three procedures were used to estimate peak pressures (defined here and in the subsequent text as the pressure at maximum temperature) and temperatures of equilibration: (i) individually calibrated thermobarometers, (ii) location of multiple reactions in P-T space using an internally consistent thermodynamic database (average P-T method) and (iii) the minimization of bulk free energies to calculate equilibrium

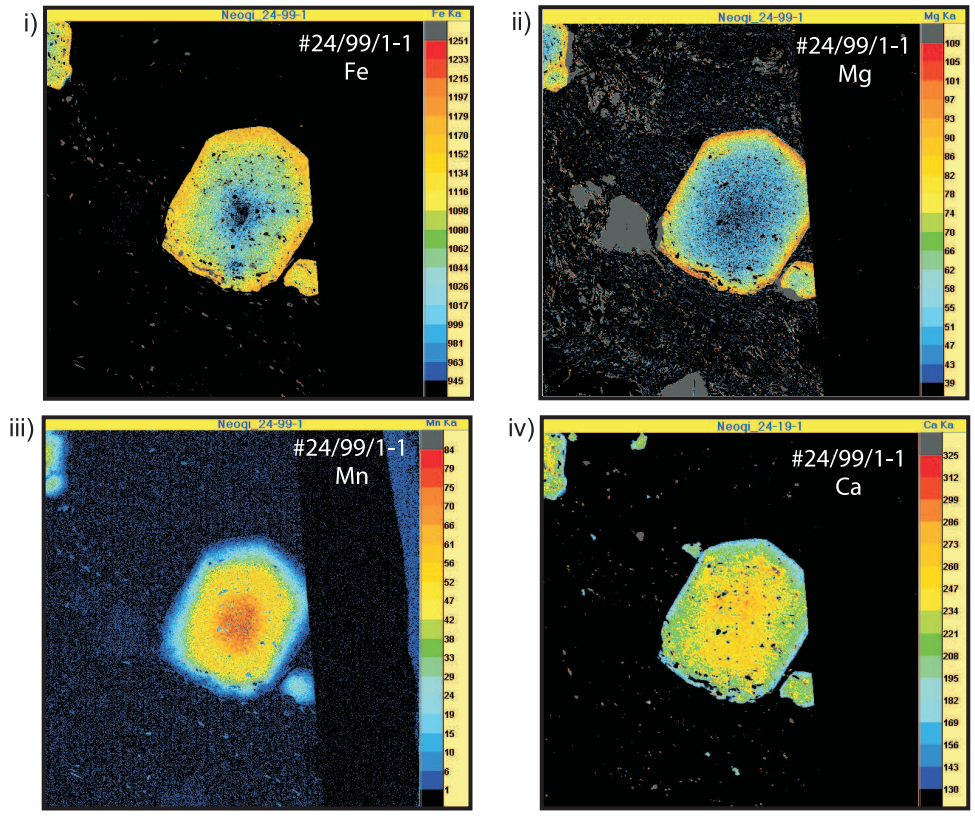

Fig. 5. X-ray maps showing element distributions in some selected garnets. The panels are arranged in the sequence (i) Fe, (ii) Mg, (iii) Mn and (iv) Ca. Color bars on the side indicate relative concentration scales. Note the locations of plagioclase and biotite from the Ca and Mg distribution maps, respectively:
(A) Garnet zone—sample #24/99/1-1,

assemblages, mineral proportions and mineral compositions (also called pseudosections). Uncertainties in reaction mechanisms and kinetics affect all of these methods to different degrees because identifying which mineral compositions were likely to represent equilibrium and should be included in the calculations to obtain the P-T conditions of interest is a problem. In addition, each of the methods have other strengths and weaknesses that have been and continue to be discussed in the literature. Therefore we applied all three methods, preferably on rocks of different bulk compositions, and evaluate the results. As the inferred metamorphic field gradients play an important role in constraining models of tectonic evolution of the Himalaya, it is worth summarizing the pros and cons of the different methods.

The individual thermobarometers suffer from errors of calibration (the location of the reaction itself as well as activity − composition models) but have the advantage that the kinetics of an individual reaction can be evaluated to estimate which mineral compositions are most likely to reflect equilibration at peak (or any other) metamorphic conditions (for example garnet rim − adjacent biotite, garnet core − included biotite, and so forth). The average P-T as well as pseudosection methods minimize the errors of individual calibrations and thermodynamic data through the use of multiple reactions in the framework of an optimized internally consistent database. But they are both subject to two problems: (i) kinetics − deciding which parts of a rock (that is,

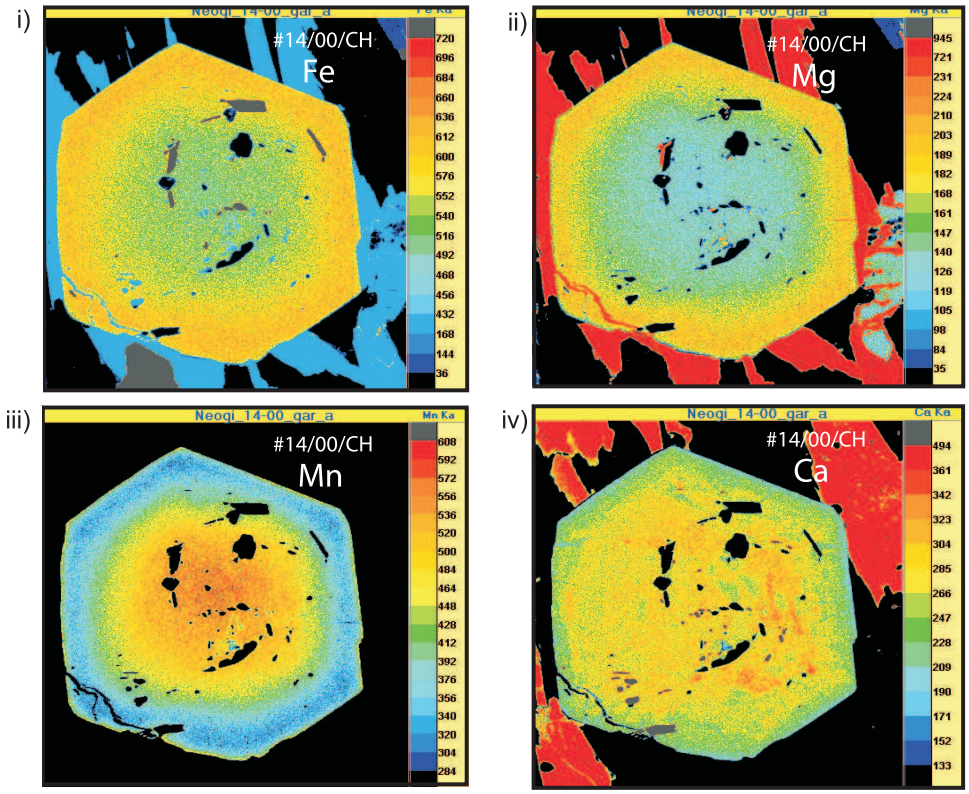

Fig. 5 (continued). (B) Staurolite zone—sample #14/00/CH. Note the very thin diffusion zoning (greenish shades) at the rim of garnet in contact with biotites in the Mg-element map and the thin Mn-rich rims (yellowish shades) in the Mn element map.

which minerals, which compositions, and how much of each phase) equilibrated at any given stage, and (ii) fluid activity − what were the activities of the fluid components, most critically H_2O, at any given stage? As a majority of the reactions considered are dehydration reactions, this effect is large. It is possible not only to shift the positions of reactions but to entirely change the topology of a phase diagram by varying fluid activities (Dasgupta and others, 2004). Finally, any open system behavior makes it difficult to identify the bulk compositions that equilibrated at any given stage of history of the rock, posing an additional problem for the pseudosection method. There have been individual attempts to get around each of these problems in specific instances. We discuss and use the method of individual thermometers and barometers first. Next, we use individual reactions to estimate fluid activities at the peak metamorphic conditions, to make better use of the average P-T and pseudosection methods.

Individual thermobarometers.—We obtained P and T using the Fe-Mg exchange equilibrium between garnet and biotite and the garnet - aluminosilicate - plagioclase - quartz (GASP) or garnet - muscovite - biotite - plagioclase (GMPB) equilibrium. We used the formulations for GASP and garnet − biotite thermometry recommended in Ganguly and others (1996) as justified by Dasgupta and others (2004). Briefly, Holdaway (2000) evaluated various garnet − biotite geothermometers and concluded that the garnet solution models of Berman (1990), Ganguly and others (1996) and Mukhopadhyay and others (1997) were roughly equivalent and the most suitable ones

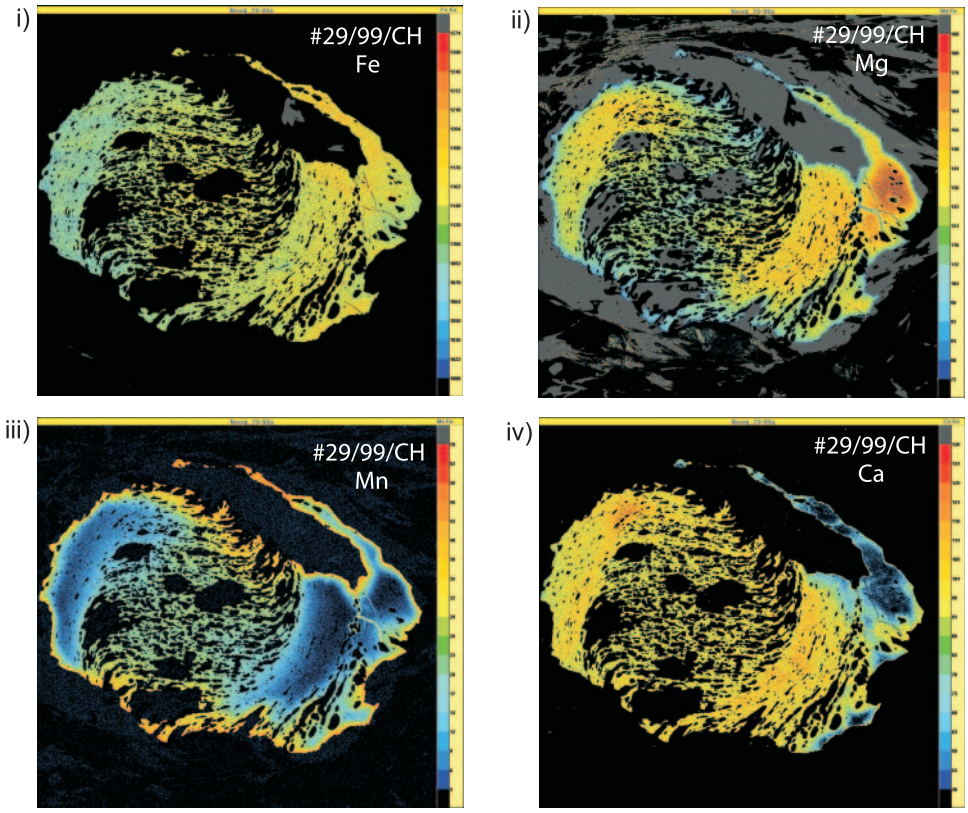

Fig. 5 (continued). (C) Sillimanite zone—sample #29/99/CH. The element distribution pattern follows the inclusion trails within the garnet. The garnet itself has been streaked out in the last phase of ductile deformation.

to use, with the qualification that the Mn−Mg interaction parameter was better constrained in the experiments and model of Ganguly and others (1996). Consequently, the Ganguly and others (1996) formulation is particularly attractive in applications to garnets with Mn-rich compositions, as is the case for some of our samples. At the highest metamorphic grades, this makes a critical difference in the P-T determinations and ultimately in the tectonic interpretation. For the GMPB barometer we have used the formulation of Hoisch (1990).

The second aspect to be considered is the choice of mineral compositions keeping kinetic constraints in mind. A commonly used strategy in the thermobarometry of a prograde sequence of rocks, notably on Himalayan samples (for example Hodges and Silverberg, 1988; Hubbard, 1989; Chamberlain and others, 1991; Hodges and others, 1993; McFarlane, 1995; Vannay and Hodges, 1996; Vannay and Grasemann, 1998; Fraser and others, 2000; Stephenson and others, 2000; Catlos and others, 2004) has been to use compositions from the same part of garnet and biotite (for example garnet rim and adjacent biotite) for samples from all grades. The simulations in Chakraborty and Ganguly (1991) demonstrate that this approach is intrinsically problematic for a sequence where rocks from different peak temperatures are considered. Up to approximately staurolite grade conditions (details depend on the actual thermal history, grain size, modal abundance of minerals, *et cetera*) growth zoning is hardly modified by diffusion, and rim compositions of garnets growing along a prograde path

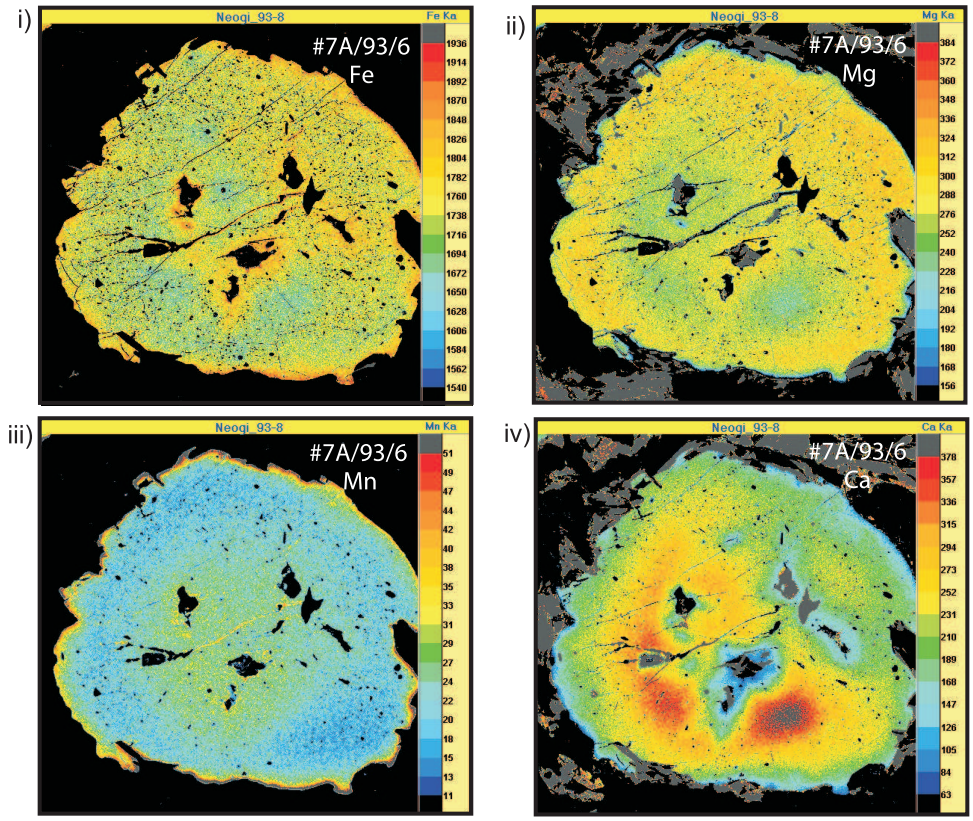

Fig. 5 (continued). (D) Sillimanite - K-feldspar zone - sample #7A/93/6. Note the coalescence of garnets that started growth from multiple nucleii. This is seen most clearly in the Ca map. Original patterns of other elements have been modified by subsequent intracrystalline diffusion, to the extent that the pattern for Mn gives the illusion of being concentric. Note the enrichment of Mn at the rim.

For the higher grade samples, the various complications in patterns, as well as the fact that the geometric cores of the crystals do not coincide with the chemical cores pose potential pitfalls for geothermobarometry if compositions are selected without element mapping.

represent equilibration at peak temperatures. At about the sillimanite zone, diffusion zoning begins to develop at the garnet rim during cooling, so that rim compositions are *not* suitable for obtaining peak temperatures. If garnets are small enough (note that the largest garnets, often chosen for analysis, are problematic in this case), they may have homogenized at peak temperatures and these compositions are most likely to be retained at the core. If there is a large reservoir of biotite in the rock (whose composition therefore does not vary much), then core garnet − matrix biotite pairs may give peak temperatures. The intermediate region in P-T space in staurolite and kyanite zones is the most problematic because compositional zoning in garnets is partially modified by diffusion and neither the core nor the rim preserves compositions from the peak temperatures. Where other sources of compositional variation (for example due to net transfer reactions) may be eliminated, compositions from near the rim, just beyond the zone affected by diffusion zoning during cooling (for example, see fig. 5B), are the closest to those attained at peak temperatures of equilibration. These may be used in combination with matrix biotite compositions in rocks with large reservoirs of biotite to get the closest approximation to peak temperatures. Compositions from no one region of garnet (core, rim) are suitable for obtaining peak

TABLE 2

Mineral reactions inferred from textural relations and chemistry

Metamorphic Grade	Bulk Composition	Textural Feature/ Compositional feature	Deduced Mineral Reactions
Biotite	Normal pelite	Lower bulk Mg content favors appearance of Bt. Chl-Ms replaced by Bt along S_2, decrease in celadonite content of Ms.	Chl + Celadonite-rich Ms ⇒ Bt +Celadonite-poor Ms + Qtz + H_2O
	Mn-rich, Grt bearing pelite	Depletion in Chl and An content of Pl in the rock, appearance of new Ms, reverse zoning in Pl.	Chl + Qtz + Bt + Pl(An-rich) ⇒ Grt + Pl(An-poor) + Ms + H_2O
Garnet	Normal pelite	Sharp depletion of modal abundance of Chl in the rock in comparison to lower grades; growth of new Bt. Favored at low fO_2 as Grt better developed in graphitic schists.	Chl + Ms + Qtz ⇒ Grt + Bt + H_2O.
	High Al-Fe pelite	Inclusion of Chl and Cld in Grt, and absence of Cld in the matrix. *Note*: Mn content of these rocks similar to normal pelites, so Fe responsible for appearance of Cld at same temeperatures as Grt appears in normal pelites (Dasgupta and others, 2004) Retrograde: Grt replaced by Chl.	Chl + Cld + quartz ⇒ Grt + H_2O
Staurolite	Normal pelite	Total elimination of primary Chl Coupled lower modal abundance of Grt	Chl + Ms +Qtz ⇒ St + Bt + H_2O Grt + Ms + Chl ⇒St + Bt + Qtz
	High Al-Fe pelite	Simultaneous appearance of St, Bt and Grt, rare preservation of Cld and Chl as inclusions in Grt, no primary Chl in matrix.	Cld + Chl + Ms ⇒ St + Grt + Bt + H_2O ; Cld + Ms + Qtz ⇒ St + Grt + Bt + H_2O
	Normal and High Al-Fe pelite	Fibrolite forms replacing Grt, Ms, Bt and Pl, fibrolite + Ilm replace Bt, syn to post S_2. Retrograde: Mica replaces St, implying mobility of K^+ and H^+. Occurrence in same thin sections as fibrolite indicates the reactions may have been coupled, leading to conservation of K+ on larger than thin section scale.	Various base leaching reactions (for example, see Vernon, 1979).

temperatures across an entire Barrovian sequence, and any attempt to do so will give inaccurate results. Using a single portion of garnet to compute P and T for all samples may account for at least part of the wide scatter of thermobarometric results reported for the IMS from the Himalaya, sometimes even from the same region (for example

TABLE 2
(continued)

Metamorphic Grade	Bulk Composition	Textural Feature/ Compositional feature	Deduced Mineral Reactions
Kyanite	Normal pelite	St inclusion in Grt, no St in the matrix, sharp mutual grain boundary between Ky and Grt, new growth of Bt	St + Ms + Qtz ⇒ Grt + Ky + Bt + H_2O or, simultaneously, St + Qtz ⇒Grt + Ky + H_2O and Ms + St + Qtz ⇒ Ky + Bt + H_2O.
	Normal pelite	Development of incipient Qtz-Pl leucosome, rarely Grt. Sharp drop of Pa content in white mica.**	Pa + Ab + Qtz + H_2O ⇒Melt, with garnet likely from the celadonite / Fe-celadonite content of the white mica.
Sillimanite-muscovite		Partial pseudomorphism of Ky by Sill (Neogi, 1993, ms.), continued presence of Ms in lower modal abundance	Ky ⇒ Sil
Sillimanite-K-feldspar		Appearance of Kfs-bearing leucosome, total elimination of primary Ms. Retrograde: replacement of Grt by Chl and Kfs by Ms.	Ms + Qtz ± Pl ⇒ Sil + Kfs + H_2O/melt.

** (i) Chatterjee (1972) demonstrated that paragonite breaks down before muscovite through reactions like paragonite + quartz = Aluminosilicate + albite +Melt/H_2O.

(ii) Spear and others (1999) suggested that in pelitic rocks containing 10–20% white mica, the reaction should produce 1-2 modal percent melt with drop in paragonite content of mica in residual rock from about 20 to 5%. In our rocks with 15–17% white mica, paragonite content drops from 17 to 9%, with production of about the predicted amount of melt.

(iii) Consideration of the P-T grid in NASH suggests (for example Chakraborty and others, 2003) that the hydrous, Al-silicate free reaction occurs first along a clockwise path above the invariant point, followed by the aluminosilicate bearing reaction paragonite + quartz = Aluminosilicate + albite +Melt/H_2O on further heating, consistent with observation.

Langthang, Nepal: Inger and Harris, 1992; MacFarlane, 1995; Fraser and others, 2000; increasing P-T with a drop of P at the highest grades: Stephenson and others, 2000; Kohn and others, 2001; Catlos and others, 2001; isothermal conditions with complex variation in pressure: Fraser and others, 2000; and nearly isobaric conditions with increase in temperature: Vannay and others, 1999). The strategy outlined here has been followed without the clarifications above in Dasgupta and others (2004), which may be consulted for examples of such application.

The results obtained from individual thermobarometers are provided in table 3 and shown in figure 6. We obtain peak P-T conditions ranging from 4.8 kbar, 490 °C (garnet grade) to 8.4 kbar, 715°C (sillimanite − K-feldspar grade) in east Sikkim and 5 kbar, 525 °C at the garnet grade to 7.9 kbar, 740 °C (sillimanite − muscovite grade) in north Sikkim. This range does not change if the Holdaway (2000) formulation of the geothermometer is used instead. In addition to zoning in garnets, there are considerable uncertainties about which biotite and plagioclase compositions to use. We have varied the biotite and plagioclase compositions over the entire range found in any

TABLE 3

Results of thermobarometery using individual thermobarometers and average P-T methods

Traverse	Sample No.	Zone	Structural Distance from Grt isograd	Individual Thermobarometer			Holland & Powell Average P-T			Berman TWQ Method	
			(km)	Equilibria used	P(kbar)	T(°C)	P(Kb)	T(°C)	Without Muscovite P (Kb)	P(Kb)	T(°C)
East Sikkim	8/00	Grt	0	GARB-GBMP	4.8	490	6.1	500	-	6.5	510
East Sikkim	11/00	St-Ky	2	GARB-GASP	5.7	550	7.7	631	-	5.8	585
East Sikkim	15/00/CH	St	3.8	GARB(GASP)	5.9	540	n.e	n.e	-	n.e	n.e
East Sikkim	17/00	St	4.3	GARB(GASP)	5.8	540	n.e.	n.e	-	n.e	n.e
East Sikkim	18/00/2	Ky	4.8	GARB-GASP	7.3	600	n.e	n.e	-	n.e	n.e
East Sikkim	19/00/1	Ky	4.8	GARB-GASP	7.3	590	8.1	600	-	8.2	645
East Sikkim	20/00	Sil-Ms	6	GARB-GASP	7.5	670	8.1	706	-	7.5	735
East Sikkim	29/00	Sil-Kfs	9.3	GARB-GASP	7.8	700	8.8	826	-	8.5	740
East Sikkim	143/01/2	Sil-Kfs	14	GARB-GASP	8.4	715	7.5	764	-	8.2	700
North Sikkim	24/99/1-1	Grt	2	GARB-(GBMP)	5	525	5	445	-	5.3	480
North Sikkim	27/99/1	Ky	13.5	GARB-GASP	6	552	6.9	625	6.3	6.2	590
North Sikkim	29/99/Ch	Sil-Ms	18	GARB-GASP	6	610	6.8	711	6.7	6.7	656

GARB: Grt-Bt-Thermometer
GASP: Grt-Als-PL-Qtz-Barometer
(GASP): mean from nearest sample
(GBMP): Grt-Pl-Bt-Musc Barometer from nearest samle
GBMP: Grt-Pl-Bt-Musc Barometer
n.e.: not enough equilibria

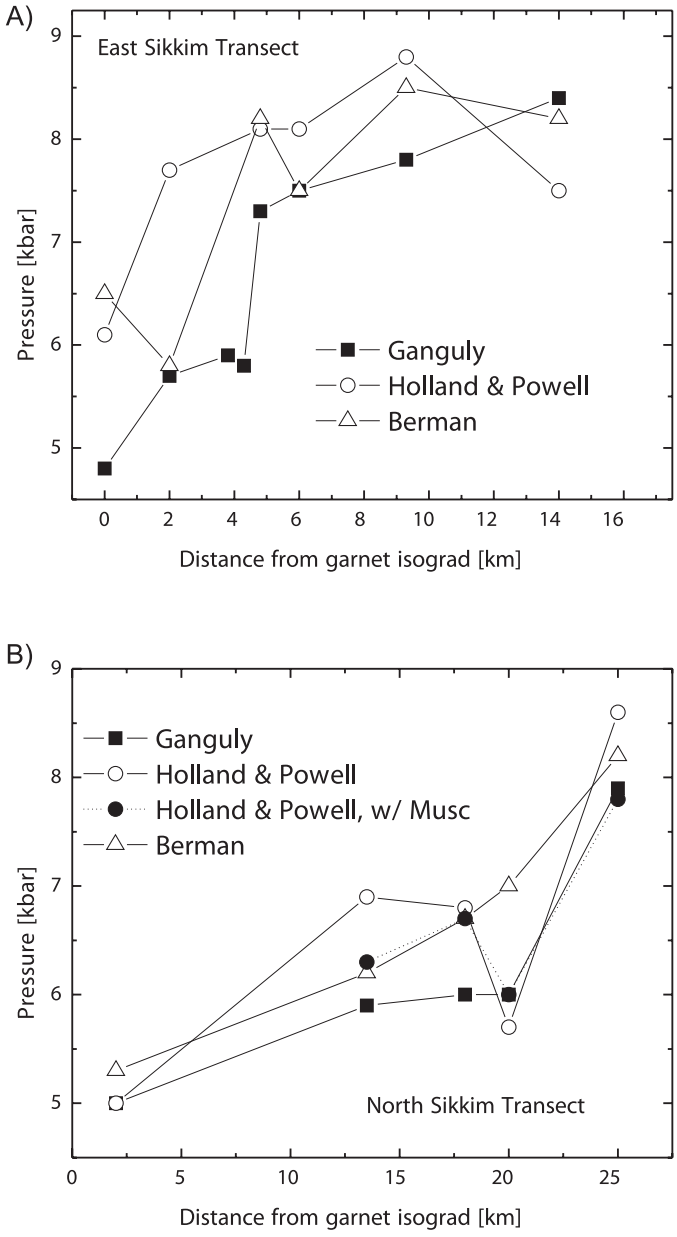

Fig. 6. (A) & (B) Variation in peak pressure (P at Tmax) with structural distance from the garnet isograd calculated with conventional geothermobarometers (filled squares), Holland and Powell Average P-T method (open circles) and Berman TWQ method (triangles). Results of calculation using the Holland and Powell method, but excluding the problematic white mica phase (see text), are shown as filled circles. (A) East Sikkim transect, (B) North Sikkim transect.

zone (Supplemental table 1, http://earth.geology.yale.edu/~ajs/SupplementaryData/2008/08DasguptaTable1.pdf) keeping the choice of garnet composition dictated by the considerations above constant. This results in a total range of ± 1.1 kbar and ± 60

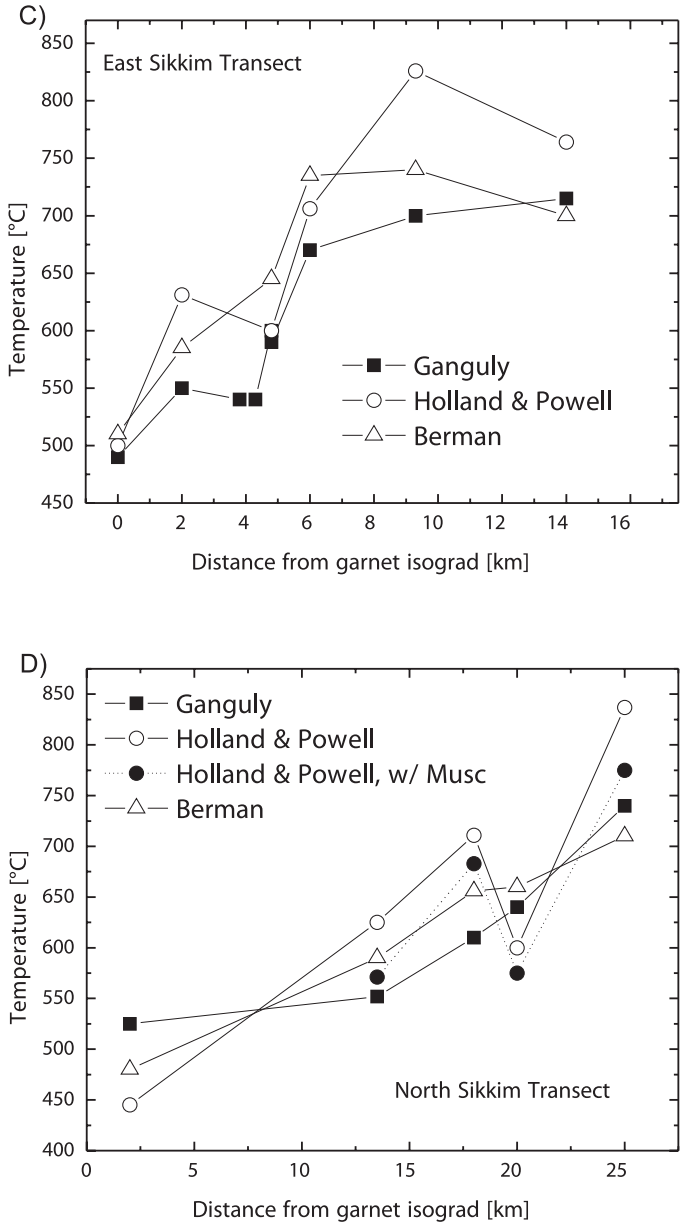

Fig. 6 (continued). (C) & (D) Variation in peak temperatature with structural distance from the garnet isograd calculated with conventional geothermobarometers (filled squares), Holland and Powell Average P-T method (circles) and Berman TWQ method (triangles). Results of calculation using the Holland and Powell method, but excluding the problematic white mica phase (see text), are shown as filled circles. (C) East Sikkim transect, (D) North Sikkim transect.

°C and there is no change in the observation that both P and T increase toward higher structural levels. The average, metamorphic field gradients in east and north Sikkim are +60 °C/kbar and +70 °C/kbar, respectively.

Activity of H_2O.—The activity of H_2O may be estimated using the equilibria (texturally corroborated)

$$23Cld + 8Qtz = 4St + 5Grt + 21H_2O$$

and

$$6St + 11Qtz = 4Grt + 23Ky + 3H_2O$$

in combination with P-T estimates of the relevant rocks (550 °C, 5.7 kbar and 590 °C, 7.2 kbar, respectively − table 3). We used measured mineral compositions, thermochemical data from Holland and Powell (1998), assumption of ideal mixing in the solids, and water fugacities from Burnham and others (1969) in equation 4.48 from Ganguly and Saxena (1987) to obtain a_{H_2O} of 0.83 and 0.89 from the two equilibria, respectively. Notwithstanding various uncertainties, the calculations show that water rich fluids with a_{H_2O} of 0.8 to 1.0 are appropriate for these rocks. We use this result as input to methods (ii) and (iii) for thermobarometry.

Average P-T method.—This method was applied using the thermodynamic database of either Holland and Powell (1998) or that of Berman (1988) (the TWQ program). The results are shown in table 3 and figure 6 and are subject to the uncertainties of reaction kinetics and a_{H_2O} noted above. We have varied a_{H_2O} from 0.5 to 1 as a conservative measure and found that the calculated P and T are both lowered, by 0.5 to 0.6 kbar and 50 to 60 °C, respectively for reduced H_2O activity. There is a close correspondence of the P-T trends obtained using the two methods and the results obtained in (i), excepting for the samples from the highest structural levels in east Sikkim. For these, lower P-T estimates than the samples at lower structural levels are obtained using both average P-T methods, similar to the observations of Stephenson and others (2000) in Zanskar Himalaya. Garnet compositions at this structural level (for example in sample 143/01) are particularly Mn rich, and problems with activity models for Mn-rich garnets have already been discussed. Further, for garnets of similar grain size there is progressively increased homogenization of compositional zoning at this structural level relative to that at immediate lower grade, implying higher temperatures were attained by these rocks. Additionally, note that this drop in P-T is not seen in the samples from north Sikkim, where the garnets are not Mn−rich at this grade. Consequently, we consider the lowering of estimated P-T at this structural level to be an artefact of the choice of mixing models and the P-T trends obtained in (i) to be more reliable in this regard.

A second observation is that calculated pressures are often higher using the Holland and Powell (1998) formulation. On inspection of the details of the calculations we found that the higher pressures stem largely from reactions involving celadonite, Fe-celadonite and eastonite components for which activity − composition relations are practically unconstrained from direct experiments. Therefore, we tested the effect of avoiding the use of these components by not using muscovite in the assemblage for which the average P-T are calculated. The results from the remaining reactions are very close to those obtained in (i) and the TWQ method of Berman. Because white micas from this region are unusually rich in the celadonite and Fe-celadonite components (Supplemental table 1, http://earth.geology.yale.edu/~ajs/SupplementaryData/2008/08DasguptaTable1.pdf), their influence on calculated P-T is larger than would commonly be the case.

Pseudosection method.—We calculated pseudosections in the MnCNKFMASH system using THERMOCALC (v. 3.21) (Powell and Holland, 1988, with data from Holland and Powell, 1998, updated 13 November 2002) for the different bulk compositional groups of our samples: (a) low Al, high Fe pelite (sample # Sin 8), (b) low Al, very high Fe pelite (sample # 7/00/R6/CH), (c) high Al, high Fe pelite (sample

#24/99/1-1), (d) high Ca pelite (sample #14/00/CH) and (e) high Mn pelite (sample #18/00/CH). We have not included Fe_2O_3 and TiO_2 components because of the uncertainties in constraining fO_2, which affects activities of these components. This implies a reduction in the stability field of biotite bearing assemblages, particularly at higher grades. The phases we have considered are quartz, chlorite, chloritoid, muscovite, biotite, garnet, staurolite, kyanite, sillimanite, plagioclase and H_2O fluid. Mixing models of solid solutions are taken from Tinkham and others (2001). Quartz, plagioclase and water were considered to be excess phases.

Figure 7 illustrates the calculated pseudosections. With the pseudosection for each bulk composition we consider the assemblages that would develop along a metamorphic field gradient of 65 °C/kbar, an average of the values inferred in section (i) above. In addition, we discuss how the calculated P-T from section (i) for rocks of different grades and bulk compositions compare with the stability fields calculated in the pseudosections.

(a) Low Al, high Fe pelite (Sample # Sin 8), figure 7A, B: Along a gradient of 65 °C/kbar starting from 450 °C, 5 kbar one encounters Chl + Bt + Ms ⇒ Grt + Chl + Bt + Ms ⇒ St + Grt + Chl + Bt + Ms ⇒ St + Grt + Bt + Ms ⇒ St + Grt + Bt + Ms + Ky ⇒ Grt + Bt + Ms + Ky/Sill (all with Qtz, Pl and H_2O). This matches very well with the observed sequence in the Sikkim metapelites. Results of geothermobarometry [(i) and (ii) above] are compared with calculated stability fields in the pseudosection ($a_{H_2O} = 1$ in fig. 7A; $a_{H_2O} = 0.8$ in fig. 7B) in table 4. We find that results obtained in (i) and (ii) are more consistent with stability fields in the pseudosection calculated with $a_{H_2O} = 0.8$ (for example, consider the location of the staurolite out reactions in fig. 7B and table 4), which is the activity of water calculated above specifically for the metamorphism of these samples. Therefore, we conclude that not only the sequence of assemblages but also the quantitative results from thermobarometry and pseudosection calculations show good agreement, providing us with a robust estimate of the metamorphic field gradient for this bulk composition across the IMS in Sikkim.

(b) Low Al, very high Fe pelite (Sample # 7/00/R6/CH), figure 7C: Along the same metamorphic field gradient as above, the following phase fields are encountered: Chl + Cld + Ms ⇒ Chl + Cld + Ms + Grt ⇒ Chl + Ms + Grt + St ⇒ Chl + Cld + Ms + Grt + Bt ⇒ Chl + Cld + Ms + Bt + St ⇒ Chl + Ms + Grt + Bt + St ⇒ Ms + Grt + Bt + St ⇒ Ms + Grt + Bt + St + Ky ⇒ Ms + Grt + Bt + Ky/Sill (all coexisting with Qtz, Pl and H_2O). Chloritoid has a large stability field (in spite of the low Al content of the bulk), with an extremely narrow region of biotite + chloritoid stability which practically fixes the temperatures at which these two minerals can coexist for fluid saturated conditions. There is a close juxtaposition of the stability fields of a number of assemblages between 550 and 575 °C, indicating small differences in free energy between these. Consequently, this is a system where any small perturbation of the energetics (for example due to deformation, nucleation kinetics) can cause the persistence/appearance of disequilibrium assemblages by overstepping. Grt zone samples 7/00/R6/CH (Chl + Cld + Ms) and 135/01 (Chl + Cld + Ms + Grt), and staurolite zone sample 11/00 (Ms + Grt + Bt + St + Ky, with included Cld in St) occur adjacent to normal pelites for which we have already obtained P-T conditions. The stability fields of these assemblages according to the pseudosection are found to be consistent with the P-T conditions and metamorphic field gradient inferred on the basis of the adjacent normal pelites; the agreement improves if a realistic reduction of a_{H_2O} is considered, as discussed above explicitly for the normal pelites.

The staurolite out reaction in this composition occurs at a very high temperature of 670 °C. However, the absence of staurolite in any bulk composition well within the sillimanite grade can be explained by a lowering of a_{H_2O} and the resulting shift of equilibrium boundaries. Indeed, the formation of melt at these grades could have

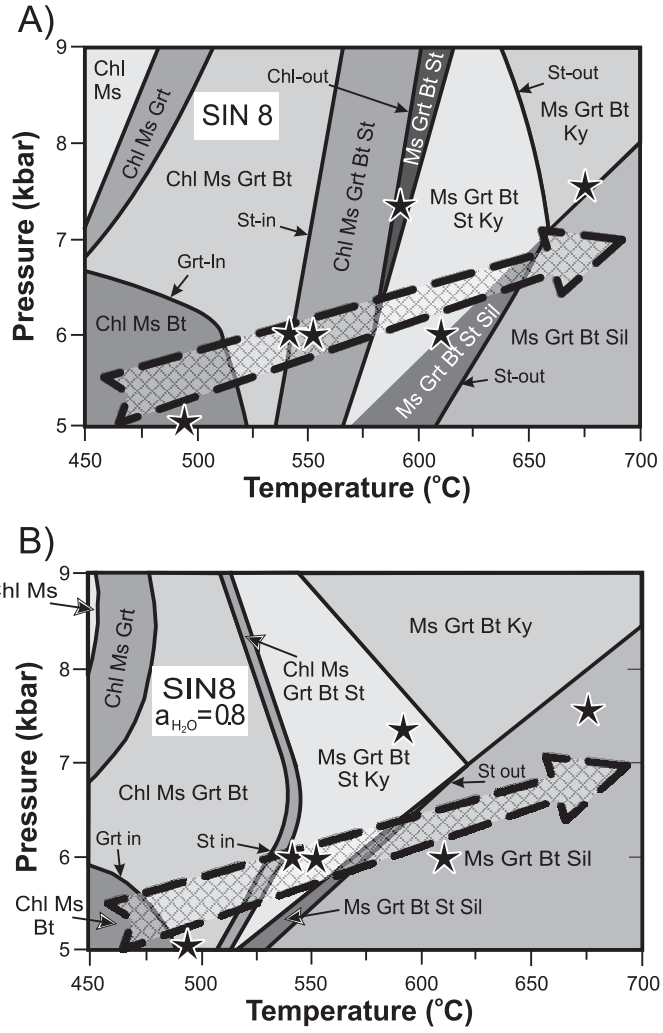

Fig. 7. Pseudosections for the system MnCNKFMASH for different pelitic bulk compositions calculated using the Thermocalc software of Holland and Powell (1998). Quartz, plagioclase and H_2O fluid are present in all fields. Note that in some cases the number of phases change by more than one between adjacent fields. In all of these cases the lower variant fields separating these "adjacent" fields are too narrow to be depicted on the scale of the diagrams, but are to be understood to be present for topological correctness.

(A) low Al, high Fe pelite (sample # SIN 8),

(B) same bulk composition as in (A), calculated for a reduced $a_{H_2O} = 0.8$,

substantially dessicated the rocks, or alternately, modified the equilibrating bulk composition.

(c) High Al, relatively high Fe pelite (Sample # 24/99/1-1), figure 7D: The topology for this composition has similarities with *(b)* in the large stability field of chloritoid (for example Wang and Spear, 1991; Droop and Harte, 1995), a narrow field of coexistence of biotite + chloritoid, and the occurrence of several closely juxtaposed stability fields at around 550 °C. It has similarities with the low Al pelite topology *(A)* at higher temperatures. The sequence of assemblages expected along the metamorphic field gradient is: Chl + Ms ⇒ Chl + Cld + Ms ⇒ Chl + Cld + St + Ms ⇒ Bt + Chl + Cld + St + Ms ⇒ Chl + Grt + St + Ms + Cld ⇒ Grt + Ms + Bt + St + Chl ⇒ Grt + Bt + Ms+

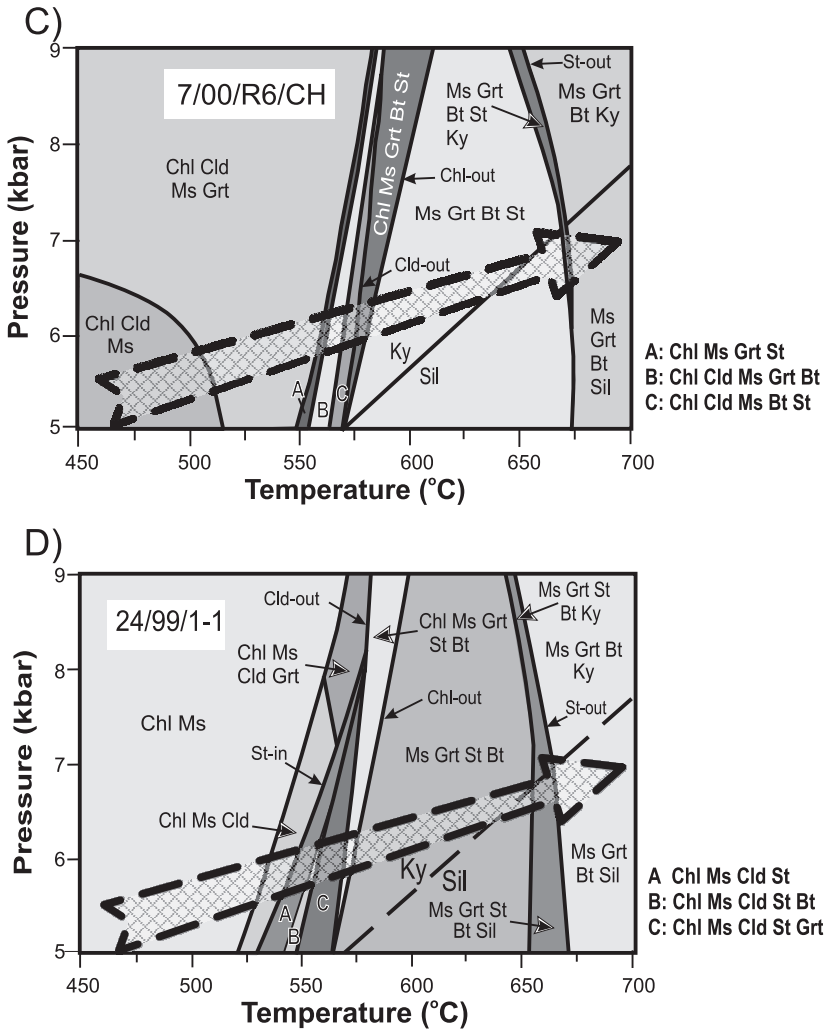

Fig. 7 (continued). (C) low Al, very high Fe pelite (sample #7/00/R6/CH), (D) high Al, relatively high Fe pelite (sample # 24/99/1-1).

St ⇒ Grt + Bt + Ms +St + Ky/Sil ⇒ Grt + Bt + Ms + Sil (all coexisting with Qtz, Pl and H_2O). The Grt-in isograd for this bulk composition lies at ~ 550°C, which is 25°C higher than that estimated from thermometry (table 3). This discrepancy may again be explained by the possible down-temperature shifting of the dehydration equilibria due to reduced water activity.

(d) Ca-rich pelite (Sample # 14/00/CH), figure 7E: The main changes in assemblages observed in this bulk composition are the appearance of garnet at lower temperature (~ 460 °C) and the appearance of staurolite at higher temperature (~ 590 °C). The suppression of staurolite stability is consistent with the conclusions of Spear and others (1995), but the extent of suppression is too large, if the results of geothermometry on this sample are considered (~ 540 °C). Shift in reaction boundaries by reducing a_{H_2O} can make results from the two approaches consistent.

(e) High Mn pelite (Sample # 18/00/CH), figure 7F: The different behavior of this bulk composition is as expected, with the appearance of garnet at lower T (445 °C, 3 Kbar)

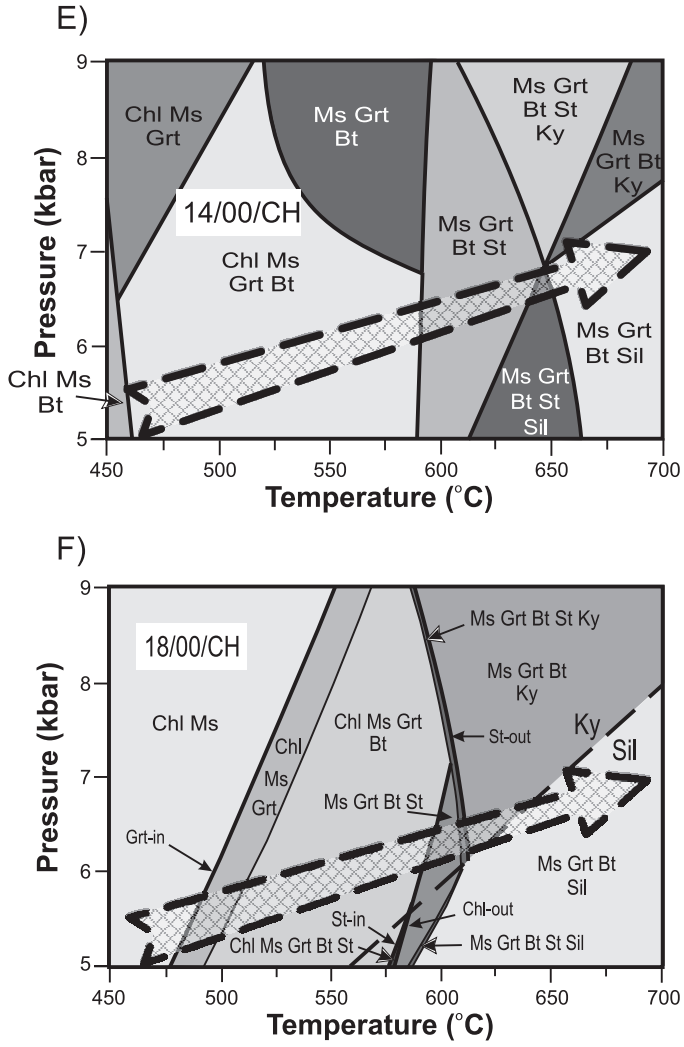

Fig. 7 (continued). (E) Ca-rich pelite (sample # 14/00/CH), (F) high Mn pelite (Sample # 18/00/CH). Figure (F) is taken from Chakraborty and others (2007), who studied the same samples.

Wide arrows across phase diagrams indicate average of the metamorphic field gradient inferred from thermobarometry in the earlier sections. As noted in the text, the gradients in east and north Sikkim are somewhat different. For any given bulk composition, the sequence of appearance of assemblages in the field can be compared to that expected along such arrows on the pseudosections; the absolute P-T values where these assemblages appear also correspond to results obtained using other methods of thermobarometry (see text). This is illustrated for the normal pelite composition (figs. 7A and 7B) using stars to denote the P-T conditions obtained from individual thermobarometry. The P-T conditions and observed mineral assemblages are more consistent with the diagram (B) drawn with reduced $a_{H_2O} = 0.8$:

- P-T for Grt grade normal pelite falls in the Grt-bearing field in 7B (it is outside in 7A)
- P-T for the Ky grade pelite (590°C, 7.3 kbar) with included St comes in the field of Ms+Bt+St+Ky+Grt in 7B (it is slightly outside in 7A)
- P-T for Sill-Ms grade pelite 29/99/CH (610°C, 6 kbar), north Sikkim, plots in the appropriate field in 7B (it is in the Ky field in 7A, although just).
- P-T for Sill-Ms grade pelite 20/00 (670 °C, 7.5 kbar), east Sikkim, plots well within the Sill field (it is on the Ky-Sill line in 7A).

The mismatch of some of the individual P-T points with the field gradient is less when the gradient for that region (north or east) is considered rather than the average.

TABLE 4

Comparison of P-T obtained from individual thermobarometers and pseudosection calculated with different a_{H_2O} for the normal pelite bulk compositional group

Compositional group, Sample # (Grade)	**Samples of the same group/appearance of index minerals**	**Independent P-T P in kb, T in ^{0}C**	**Average P-T (Holland & Powell)**	**Range in T according to pseudosection at P of interest (*T at P of interest in the pseudosection at a H_2O = 0.8, fig. 7B)**
Normal pelite, #Sin8 (Ky), fig. 7A	Grt–in isograd, #8/00 (east Sikkim)	4.8, 490	6.1, 500	520-530 at 5 kb (*485-510 at 5 kb)
	St grade, #15/00/CH, #17/00 (east Sikkim)	5.8-5.9, 540	Not enough equilibria	540-565 at 6 kb (*530-535 at 5 kb)
	Ky grade, #19/00/1 (east Sikkim)	7.3, 590	8.1, 600	575-630 at 7 kb (*535-600 at 7 kb)
	Ky grade #27/99/1 (north Sikkim)	6, 552	6.9, 625	565-625 at 6 kb (*540-570 at 6 kb)
	Sill-Ms grade, #20/00 (east Sikkim)	7.5, 670	8.1, 706	>675 at 7.5 kb (*>640 at 7.5 kb)
	Sill-Ms grade, #29/99/CH (north Sikkim)	6, 610	6.8, 711	>625 at 6 kb (*>570 at 6 kb)

as already found in the pseudosection calculations of Mahar and others (1997) and Wei and others (2004). This explains the occurrence of the spessartine rich garnet bearing sample #1C/00/3 within the biotite zone defined on the basis of assemblages in normal pelites. The kyanite zone Mn−rich sample #18/00/CH (Grt + Bt + Ms + Ky + Pl), estimated to have equilibrated at 590 °C and 7.3 kbar on the basis of thermobarometry, has the appropriate stability field in the pseudosection at this P-T condition. Pseudosection results obtained on the adjacent (same outcrop) low Al pelite #19/00 (Chakraborty and others, 2007) are also consistent with this P-T condition.

Considering results from all the pseudosection calculations, the few mismatches between results from pseudosection calculations and individual thermobarometers are all in the same direction: pseudosections indicate higher temperatures. This is expected, considering that most of the pseudosections have been calculated for $a_{H_2O} = 1$. Entirely independent of the calculations we have performed above, there is no reason to expect fluids present during the metamorphic reactions to have been pure H_2O. As shown with one example of a pseudosection calculated at a lower a_{H_2O} ($a_{H_2O} = 0.8$, fig. 7B), agreement improves between the two if realistic, lower a_{H_2O} are used for computing pseudosections. A second point is that all the mismatches occur in samples from the N Sikkim traverse, suggesting perhaps that metamorphism of rocks in this area occured under lower a_{H_2O}, generally speaking.

MASS TRANSFER AND OPEN SYSTEM BEHAVIOR

Equilibrium phase relations in given bulk compositions can explain observed mineral assemblages in the metamorphic sequence. When different assemblages are observed in adjacent rocks, bulk chemical analyses provide plausible explanations based on variations in the topology of phase diagrams. Nevertheless, no metamorphic system with widespread dehydration reactions is a closed system and in this section we evaluate the degree and nature of mobility of elements. The consistency of chemical and mineralogical data indicates that the bulk compositions determined here are representative and therefore they can be used to study mobility of elements with confidence. We use the statistical and graphical approach based on conservation of mass developed by Brimhall and others (1988) and Ague (1991, 1994a, 1994b).

The main dilemma in assessing element mobility from an analysis of compositional variations is the well known petrological source vs. process problem: separation of the effects of protolith variability from those due to element mobility. The method of Brimhall and others (1988) and Ague (1991) tests the hypothesis that observed compositional variations are caused by element mobility. Issues central to the meaningful application of the method are the choice of a suitable reference element and the size and spacing of sampling, which determines the length scale on which element mobility is evaluated. Good reference elements should have low concentrations and variability in metamorphic fluids across the P-T range of interest. After evaluating our data following the procedure in Ague (1994a), we have chosen Ti as the reference element so that our plots and results are directly comparable to those of Ague (1994a).

To aid interpretation of the diagrams that follow, we depict in figures 8A and 8B (adapted from fig. 4 in Ague, 1994a) the different trends expected due to element gain or loss. Figures 8C–8G show plots, against Ti (or TiO_2 for major elements), for various other candidates for reference elements (Al, Fe, Zr, Nb and Ni). In these and other plots that follow, dashed lines show the corresponding areas where data from Ague (1994a) would plot. We find that chlorite − biotite grade "protoliths" from this study cluster over slightly wider ranges than in the study of Ague (1994a), particularly for Al_2O_3. However, a significant number of higher grade samples also fall within the same clusters. This suggests that the overall variability of bulk compositions/protoliths is larger in this area compared to the Weepawaug schists studied by Ague (1994a). However, the overall compositional range spanned by the rocks from Sikkim, when all grades are considered, are narrower. Secondly, there is a slight trend of residual dilution (= addition of some mobile elements), rather than the residual enrichment observed by Ague (1994a, 1994b). Finally, Fe_2O_3 appears to have been quite mobile and is not an appropriate reference element for the present set of samples.

Figures 9A–9F shows plots of potentially mobile components SiO_2, Na_2O, CaO, MnO, MgO and K_2O, all with respect to TiO_2. Considering the chlorite − biotite grade rocks to have been the protolith, we find that SiO_2 is clearly a mobile component that has been *added* to the higher grade rocks. For other elements, a significant number of higher grade samples plot within the field of protoliths, suggesting limited overall mobility. However, the mobility trends that are observed are different for different elements: no change or mass gain for SiO_2, gain/no change for Na_2O, no change for MgO, gain/no change for CaO, no change/loss for K_2O and gain/no change for MnO. The suggested gain/loss can be further evaluated using the statistical mass balance calculations proposed by Ague (1991, 1994a). He defines a variable τ_{Ti}^{i} as $[(C_{Ti}^{o}/C_{Ti}^{'}) \times (C_i^{'}/C_i^{o}) - 1] \times 100$, where C_{Ti}^{o} and $C_{Ti}^{'}$ are the concentration of Ti in the initial and final states respectively, and Ci^{o} and C'_i are the same for the mobile element. Computation of τ_{Ti}^{Si}, τ_{Ti}^{Na}, τ_{Ti}^{Ca}, τ_{Ti}^{Mn}, τ_{Ti}^{K} and τ_{Ti}^{P} values using the chlorite − biotite grade rocks as putative protoliths (table 5) reveals small values of τ_{Ti}^{i} indicating low overall mobility of elements with only occasional exceptions. Interestingly, these exceptions (for example #18/00 and #19/00 from a kyanite grade outcrop in east

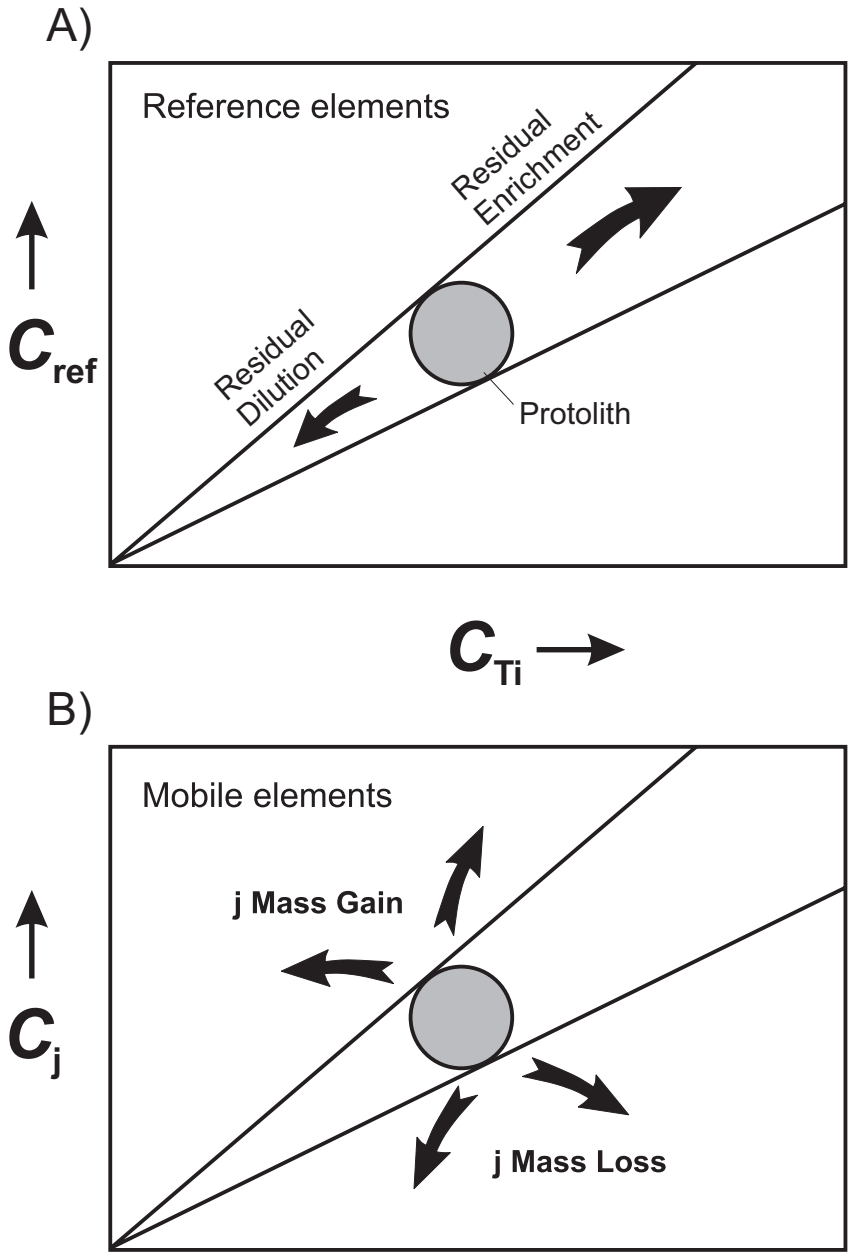

Fig. 8. (A) & (B) Expected vectors for residual enrichment/depletion of reference elements (A) and mass gain/loss of mobile elements (B) with respect to a reference element, chosen to be Ti. The gray shaded region indicates the composition of a hypothetical protolith. The figure is adapted from figure 4 in Ague (1994a).

Sikkim) are invariably for rocks from outcrops showing an increased abundance of quartz veins and other evidence of local, enhanced fluid activity (a listing of different lines of evidence may be found in Chakraborty and others, 2007). The τ_{Ti}^{i} values indicate mass gain of SiO_2, CaO and Na_2O (particularly at the higher grades) and

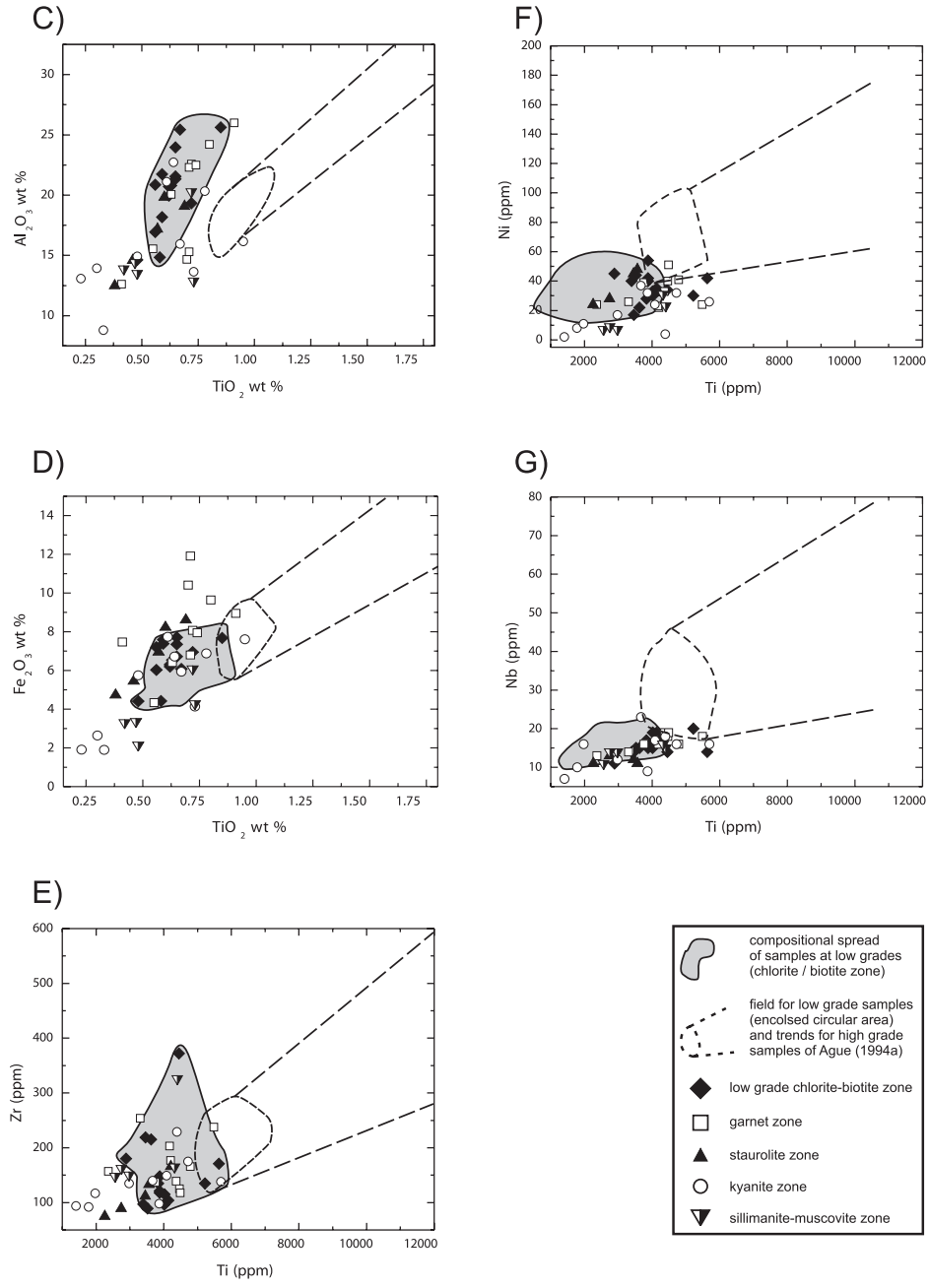

Fig. 8. (continued). (C)–(G) Test of various elements as possible candidates for immobile, reference species against variation in Ti content of the bulk rock samples. (C) TiO_2 wt.% vs. Al_2O_3 wt.%, (D) TiO_2 wt.% vs. Fe_2O_3 wt.%, (E) Ti (ppm) vs. Zr (ppm), (F) Ti (ppm) vs. Ni (ppm), and (G) Ti (ppm) vs. Nb (ppm). Symbols used in this diagram are as follows: filled diamonds: low grade chlorite-biotite zone, square: garnet zone, filled triangle: staurolite zone, circle: kyanite zone, and inverted half-filled triangle: sillimanite-muscovite zone. Shaded area in this figure as well as in figure 9: compositional spread of samples at low grades (chlorite/biotite zone). Dashed lines indicate the field for low grade samples (enclosed circular area) as well as trends for high grade samples of Ague (1994a).

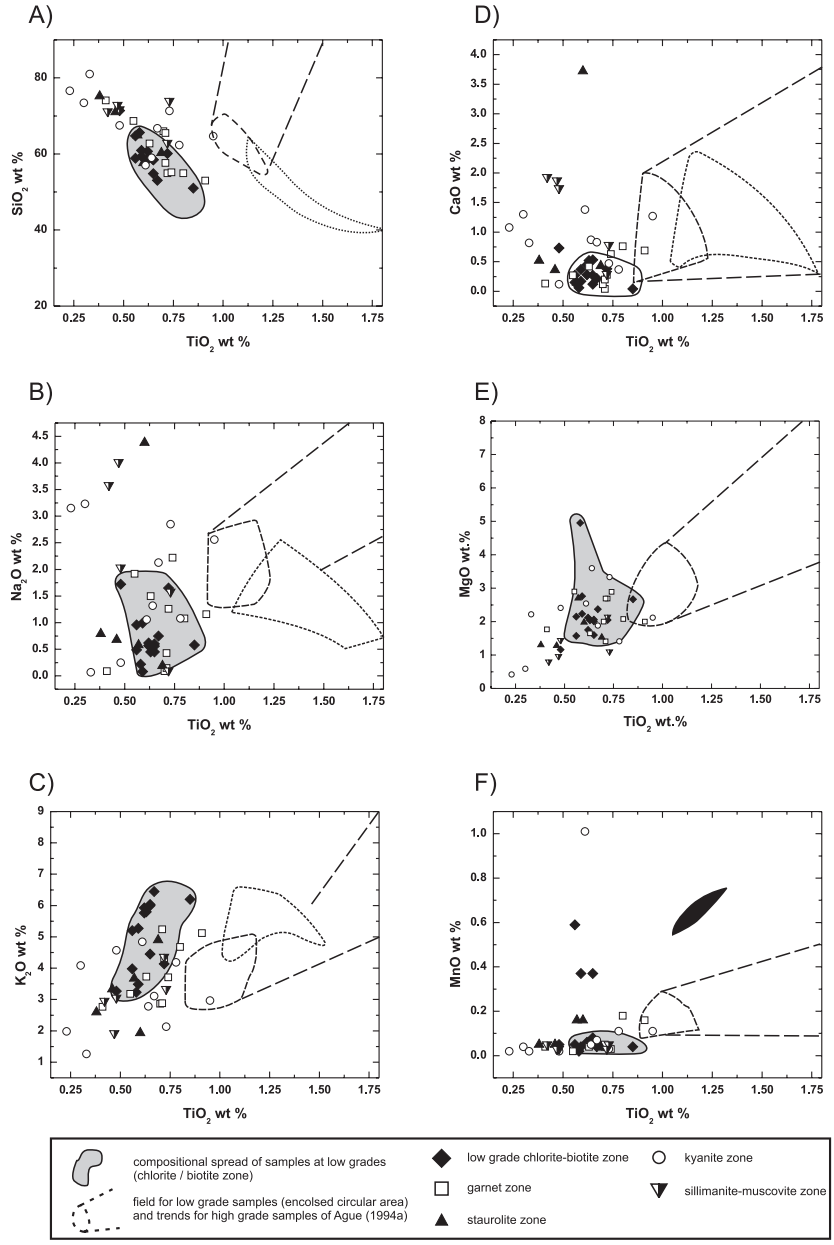

Fig. 9. Test of major element mobility with Ti as the reference species: bulk compositional plots of TiO_2 versus (A) SiO_2, (B) Na_2O, (C) K_2O, (D) CaO, (E) MgO, (F) MnO. Symbols, shaded area and dashed lines are the same as described in the caption for figure 8. The striped area in panel (F) is the location of unusually Mn rich samples of Ague (1994a), note that similar Mn rich samples occur in our study area too, at corresponding Ti contents. The areas marked by dashed and dotted lines are the areas where the low and high grade samples of Ague (1994a) plot, respectively.

significant mass loss of K_2O. Mn is interesting in that depending on the choice of protolith, Mn may have been gained, lost or conserved during metamorphism.

Because Zr follows SiO_2 during clastic sedimentation, there is a strong positive correlation in sedimentary rocks between these two that is destroyed if SiO_2 is

TABLE 5

Percentage of mass change computed with respect to average Chlorite-Biotite zone protholith using Ti as reference element

	τ Ti_Si	τ Ti_Al	τ Ti_Fe	τ Ti_Mn	τ Ti_Mg	τ Ti_Ca	τ Ti_Na	τ Ti_K	τ Ti_P
Grt zone									
24/99/1	-28.18	-7.39	14.34	6.36	-27.31	97.60	18.98	-27.22	-47.33
24/99/1 (2^{nd} sample)	-39.22	-12.86	-6.91	-17.09	-38.71	57.32	12.07	-30.18	-54.00
158/00/1	-20.43	-4.32	6.03	-73.82	4.13	-19.36	53.76	-25.59	-19.33
8/00	-15.37	-4.20	-9.42	-73.45	5.58	-88.32	-46.80	-8.49	-55.50
19/99/CH	31.24	-13.10	-24.76	-82.73	48.12	2.60	209.15	-27.73	-52.08
24/99/CH	4.76	-2.01	-2.91	-69.82	-26.37	39.44	111.02	-25.94	-16.67
8/00/CH	-1.79	-36.10	40.57	-73.09	-20.43	-64.48	-88.71	-49.19	5.00
158/01/CH	-22.31	-7.39	1.55	-80.91	8.76	76.40	163.39	-37.87	-29.17
7/00/R6/CH	-3.82	-34.26	58.66	-66.82	-44.66	-41.60	-81.44	-49.70	3.83
7/00/R4/CH	89.16	-5.80	73.12	-53.82	20.85	-33.96	-80.63	-15.84	2.67
St zone									
17/00	18.80	-8.04	15.41	32.36	32.10	-45.40	-10.54	-20.10	-16.75
14/00/CH	0.84	1.48	30.66	26.55	-7.39	1194.56	545.86	-59.83	13.75
17/00/CH	-9.10	-15.82	17.84	-72.73	-38.31	29.00	-75.85	-12.08	-24.17
16/00/CH	107.25	0.74	18.25	-37.73	-4.25	184.96	83.44	-14.78	66.00
15/00/CH	61.47	-3.09	12.38	-48.64	-22.24	62.72	30.24	-9.98	25.58
Ky zone									
18/00/2	-16.01	-19.88	-15.88	-33.00	-49.21	-0.84	22.64	-32.84	-66.25
Sin8	-28.45	-47.69	-23.62	-45.00	-37.31	179.40	138.64	-60.92	-17.50
Sin5	1.85	-43.03	-46.36	-80.64	27.11	33.48	242.97	-63.82	-6.83
19/00/02	248.20	73.89	-21.23	-58.91	-48.97	876.32	1106.61	7.05	105.50
19/00/1	-3.93	8.30	-0.67	-63.18	56.77	181.88	81.22	-46.13	-10.17
27/99/3	46.66	-5.21	13.32	-80.36	39.94	-48.16	-54.24	18.08	-67.25
27/99/1	4.66	-26.82	-15.45	-50.36	-21.16	158.96	181.59	-41.97	-13.83
19/00/1/CH	155.55	41.86	-16.66	-37.09	-45.12	799.60	847.10	69.28	145.00
18/00/CH	-2.45	5.55	20.05	680.45	16.08	369.20	52.71	-1.58	11.58
19/00/02	157.45	-18.21	-45.22	-71.27	88.58	418.24	-81.25	-52.37	43.25
L1/CH	61.01	-22.18	-23.79	-90.36	11.70	213.76	-85.63	-51.56	-3.25
Sil-Mus zone									
M-4/1	55.65	-14.30	-57.82	-70.55	-16.39	651.68	271.59	-21.20	41.92
M-1/2	77.36	1.17	-25.33	-43.64	-46.67	857.28	652.41	-12.49	25.00
20/00	5.54	-46.29	-44.55	-67.73	-58.01	121.52	90.14	-43.44	-71.33
29/99/CH	-9.00	-14.15	-20.12	-80.36	-17.16	-16.48	-87.80	-24.90	-12.00
25/00/CH	62.58	-5.98	-31.94	-69.73	-42.71	730.28	654.42	-49.01	89.83

mobilized during metamorphism. Indeed there is a shift in compositions to the high SiO_2 side of such a correlation trend, consistent with the inferred addition of SiO_2 during metamorphism (fig. 10, see also Moss and others, 1996; Breeding and Ague, 2002).

Finally, the similarity of grain densities (2.798 − 2.83 gm/cc) calculated for selected samples from the biotite to the kyanite zone using the modal abundances of the constituent phases in each rock, chemical composition of the phases and molar volume data (Holland and Powell, 1998) is consistent with the limited mobility inferred above.

Whether the relatively limited variation of composition across grades, as opposed to the considerable variations within a given grade, is the result of sedimentary/

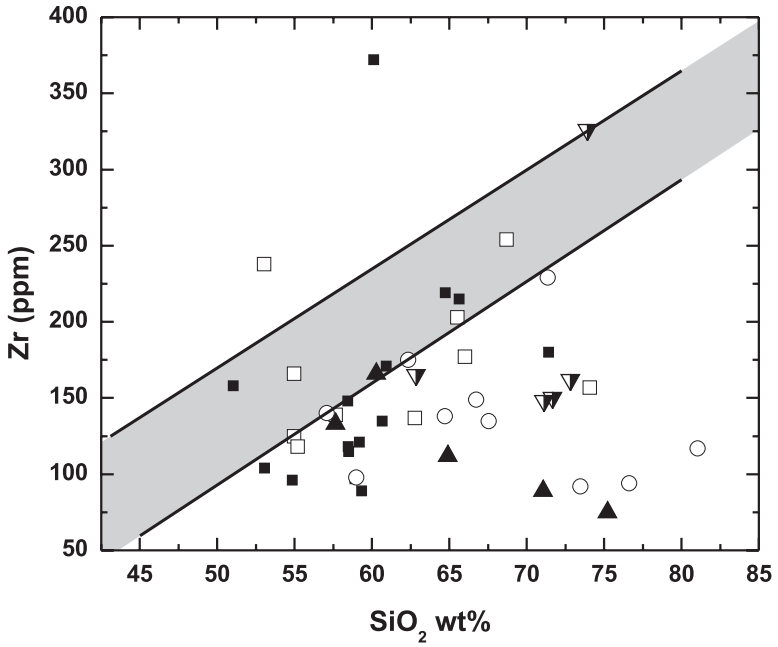

Fig. 10. Variation of Zr with SiO_2 content in the pelitic rocks of this study. Relative to the clastic sedimentary trend (shaded area) from Moss and other, 1996, the rocks of this study are more SiO_2 rich.

diagenetic or metamorphic processes may be assessed by comparing compositions with average shales and slates in plots of ln (SiO_2/TiO_2) vs. ln (SiO_2/Al_2O_3). Similarly, plots of ln (X/SiO_2) or ln (X'/Ti) where X = components such as Na_2O, K_2O, CaO, X' = Zr, Sr for the lower grade protoliths from Weepawaug schists show a constant trend, whereas the higher grade rocks show a trend of increase/decrease depending on mass gain or loss during metamorphism (for example Ague, 1994a). The corresponding plots of data from Sikkim (Supplemental table 1, http://earth.geology.yale.edu/~ajs/SupplementaryData/2008/08DasguptaTable1.pdf, plots not shown) reveal that while there is considerable overlap in composition between shales/slates and the lower grade rocks, many higher grade rocks plot in the same area as well corroborating once again generally limited element mobility.

In combination, the calculations and plots indicate that the overall mobility of elements during metamorphism of the Himalayan metapelites in Sikkim was relatively low at scales larger than hand specimens, consistent with earlier inferences from phase equilibria. The lower as well as the higher grade rocks have compositional counterparts in the shale/slate groups. The mobility that has occured, however, has resulted in a net mass gain, mainly in the form of SiO_2, relative to the lower grade rocks. We note in this connection that most inferred model reactions in table 2 have quartz (that is, the SiO_2 component) as a reactant that is consumed. Other mobility trends include gain of Na_2O, CaO and possibly Fe_2O_3; and loss of K_2O. This is analogous to the behavior observed by Breeding and Ague (2002) in the Otago schists of New Zealand. Samples from kyanite zone and higher grades show the highest mobility, coincident with the first appearance of melts in the system. Overall limited mobility of elements found here is also consistent with the observation of much smaller amounts of quartz veins compared to the 20 to 30 percent of an outcrop that was observed at amphibolite facies conditions by Breeding and Ague (2002). Ague (1994b) showed in his study area that the growth of key index minerals such as kyanite and staurolite were related to

development of quartz veins that acted as fluid conduits. These aluminous minerals occured in zones around the quartz veins due to decrease in Na/Al and K/Al by fluid activity. We have also observed the development of coarse plagioclase close to a vein similar to the situation described by Ague (1997), but this is not the regional pattern in this area. In Sikkim the development of aluminous index minerals was primarily controlled by variations in P-T conditions of intermingled protoliths of different bulk compositions.

TECTONIC IMPLICATIONS

The combined analysis of the role of bulk composition in stabilizing minerals, the limited role of fluid flow in modifying these bulk compositions, and the various approaches for determining pressures and temperatures of equilibration lead to the robust conclusion that the metamorphic field gradient along two different traverses in the Sikkim Himalaya is continuous and positive, that is, pressure as well as temperature increase to higher grades. This observation may now be used to evaluate possible models of the origin of IMS in the Sikkim Himalaya. We have schematically illustrated the various models in figure 11. There are in essence two classes of models for the development of IMS − those in which rocks are heated from the top (for example thrusting of hotter deeply buried crust above, either in one or in multiple steps) and those in which a right way down metamorphic pile (hotter rocks at greater depths) is inverted during or after metamorphism. Our results (fig. 6) eliminate the first class of models (expectation for metamorphic field gradient: increase of T accompanied by decrease of P) at the outset (fig. 11A). The second class of model has many variants, some of which require pieces of a right side down metamorphic sequence to be thrusted up, layer by layer, to ultimately invert the entire sequence (for example, Jain and Manickavasagam, 1993; Hubbard, 1996; Grujic and others, 1996). Our observation that the metamorphic field gradient is continuous, even when several bulk compositions are considered in parallel, renders this scenario implausible because it is difficult to envisage any kind of thrusting or other mechanical movement that disrupts a sequence, exhumes it and puts it back together in perfect order (fig. 11B). Out of sequence thrusting is commonplace in other levels and regions of the Himalaya where physical evidence of thrusting is present. It is difficult to contemplate how repeated thrust movements across this entire metamorphic zone would fail to produce a single metamorphic assemblage that is out of sequence after several bulk compositions and two different traverses have been considered. We also note here that although rocks showing pronounced flattening and deformation textures of quartz may be found locally, the vast majority of the pelites show a texture that show relatively well annealed quartz grains (for example fig. 3) and even well developed foam textures are not uncommon. This is unlikely if each layer of the sequence has been produced by thrusting. This is apparently quite different from the textures observed in similar rocks in Nepal (as illustrated, for example, in Hubbard, 1996) or the Zanskar Himalaya (Stephenson and others, 2000).

Additional constraints come from ages determined from monazite grains included in garnets and other porphyroblasts (for example, staurolites) (Catlos and others, 2001, 2004). In the Annapurna region of central Nepal a remarkable regularity of decreasing ages from 22 Ma to 3.3 Ma was observed with decreasing structural levels. This prompted Robinson and others (2003) to propose a model where metamorphism occurs in multiple stages, as successive thrust slices are accreted to the base of a propagating thrust (fig. 11C). Johnson and Harley (2003) have questioned the thermal feasibility of this model. Our observations also suggest that such a scenario is implausible in Sikkim for the same reasons as the ones discussed above for other thrusting models. However, it is interesting to note that the geochronology in Sikkim to date (Catlos and others, 2004; Dubey and others, 2005) reveals that although the general

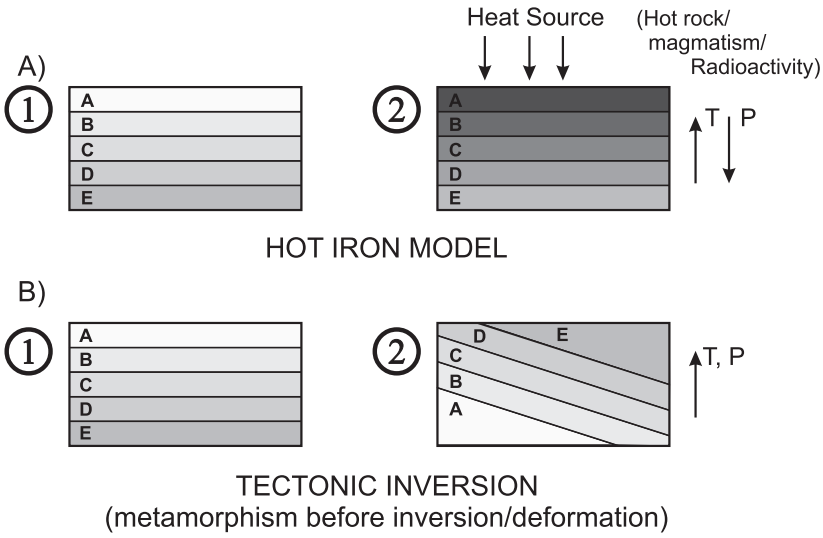

Fig. 11. Schematic summary diagram of various tectonic models that have been suggested for the generation of the inverted metamorphic sequence in different sections of the Himalaya. Numbers 1, 2, 3 *etc.* denote the sequence of events in a given model. Darker shades indicate higher metamorphic temperatures. In each case, the expected direction in which the recorded P, T and age (if applicable) are expected to increase are also shown.

(A) The so called "hot iron" model where a heat source at the top causes a regional contact metamorphism. In this scenario one would expect increasing T in the direction of decreasing P. This has not been supported by subsequent thermobarometric studies.

(B) Tectonic inversion models. In this category belong various forms of thrusting, folding and other mechanical processes that invert an already existing "right side down" sequence. The expected P, T array is consistent with observation. The suggestion of recumbent folding has been discounted because nowhere has the right side up limb of such a fold been found, and it is unlikely that this has been systematically eroded away everywhere. The various thrusting scenarios have difficulty explaining the metamorphic coherence of the sequence that is shown, for example, in this work.

trend of younging at lower grades is present, the overall spread of ages is much smaller and the pattern is not as systematic as in Nepal. Therefore, based on the monazite ages as well, a model such as that of Robinson and others (2003) would not be appropriate for Sikkim.

Our observations indicate that a right side down metamorphic sequence (increasing P with increasing T) was formed first and subsequently was inverted and exhumed (fig. 11D). We do not have any evidence in Sikkim, unlike in areas such as the Kishtwar Window in the Zanskar Himalaya (Stephenson and others, 2000), that the rocks of the IMS were pervasively sheared, as might be expected if repeated thrusting were responsible for the inversion and exhumation. Indeed, the relatively undeformed textures point strongly to strain partitioning whereby the motion of exhumation is focussed along bounding thrusts leaving the interiors of such blocks relatively undeformed, as is the situation in N Pakistan (Treloar and others, 1989). In combination with the coherence of the metamorphic sequence, this requires inversion and exhumation of a right side down sequence as a block, rather than by repeated thrusting. This is precisely the scenario predicted by the newest generation of channel flow models (Beaumont and others, 2006; Jamieson and others, 2006; Faccenda and others, 2008). While inversion of a right side down sequence occurs as an inevitable consequence of collision in all of these models, it is not clear if high enough peak temperatures were attained and if the coherence of the sequence during exhumation is guaranteed in all cases. Indeed, a general unresolved question about Barrovian metamorphism is the source of heat, as has been eloquently discussed by Jamieson and others (1998).

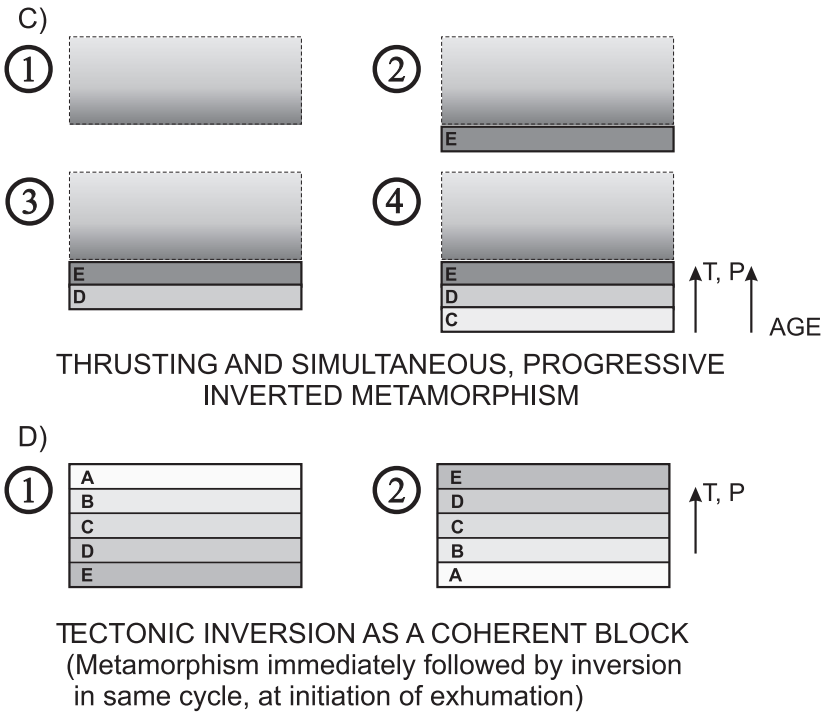

Fig. 11 (continued). (C) Models analogous to (B), but where progressively lower grades of metamorphism are produced at later times, at the sole of a propagating fold-thrust system. In this model, at each successive point of time (panels 1, 2, 3, 4), the entire block as a whole moves to shallower depths as part of a fold-thrust system. This explains the decrease in T as well as P at successive stages of metamorphism, in contrast to the static hot iron model above (A). This model produces a metamorphic age gradient in addition to gradients in P and T. This model, suggested on the basis of observations in Nepal, is also unlikely to produce a metamorphically continuous and coherent sequence such as the one found in Sikkim.

(D) A right side down "normal" metamorphic sequence is inverted in the same metamorphic cycle (at initiation of exhumation triggered by melting, for example) as a block, and exhumed by motion focussed along bounding faults with little internal deformation. This is the model that best explains the observations in Sikkim, and is consistent with recent geodynamic models of exhumation triggered by melting (for example Faccenda and others, 2008).

The numerical calculations of Faccenda and others (2006, 2008) explored the thermal and dynamic effects of different amounts of heat generation in the pieces of crust undergoing collision. This aspect of their study was motivated by the observation of unusually high concentration of heat generating elements (in particular Th) in Himalayan metapelites from all metamorphic grades and from different regions along the strike of the mountain chain ($\sim 4 - 5\ \mu W/m^3$, as opposed to mean upper crustal values of $1-2\ \mu W/m^3$). Notably, concentrations of U, Th and K from all of the samples considered in this study were a part of that database. They found that the combined heat sources of thrusting, shear heating and heat generation from the burial of such highly radiogenic sediments are capable of producing peak metamorphic temperatures up to those required for partial melting of pelites. Although the models of Faccenda and others (2008) are generic for collision systems and not tailored to the specifics of the Himalayan belt, this provides a possible solution to the heat budget problem. It is noteworthy that the timescales of burial, heating/metamorphism and subsequent exhumation found in the simulations are well within the limits permitted by the boundary conditions of the Himalayan orogeny ($20 - 30$ Myrs).

The inclusion of partial melting in the Faccenda and others (2008) model provides a simple and obvious mechanism that triggers exhumation. The reduction of

density and viscosity of a buried layer on initiation of partial melting provides a driving force for uplift and exhumation. In 75 simulations spanning a range of parameters, Faccenda and others (2008) consistently observed that the Barrovian metamorphic sequence is inverted as well during such exhumation, and in each case the exhumation of the unmelted part of the metamorphic sequence occured as a coherent block. Indeed, their results suggest that inverted metamorphic sequences may well be the rule rather than the exception, at least once melting occurs in a metamorphic pile. In any case, this is consistent with our petrological observations (positive metamorphic field gradient and petrological coherence) on the rocks from the lesser Himalaya in the Sikkim region. It is interesting to note that on entirely structural grounds, partial melting has been invoked as a triggering agent for exhumation in the adjacent Bhutan Himalaya (Davidson and others, 1997; Daniel and others, 2003) as well as in other regions (for example, see Teyssier and Whitney, 2002).

In contrast to the coherence of the unmelted part of the sequence, higher grade rocks with pronounced melting and migmatization are found to be mixed from different depths in the simulations (Faccenda and others, 2008). The shape of the P-T paths are also different, with an initial phase of rapid decompression to mid-crustal depths. Such P-T-t paths have also been documented in the higher Himalayan rocks from Sikkim (Ganguly and others, 2000; Harris and others, 2004). The extent and nature of mixing needs to be clarified through detailed studies of the higher Himalayan crystalline rocks from Sikkim. Nevertheless, it is encouraging that a generic model of subduction − collision is able to capture so much of the behavior of this key orogenic belt.

Faccenda and others (2008) did not consider at least three factors in their model that must play key roles in the evolution of the Himalayan orogen: (i) The role of dehydration reactions in reducing the rheological coupling between plates, (ii) the role of erosion in the exhumation process (see, for example, Beamount and others, 2006, for the importance of this parameter), and most importantly, (iii) in their large scale model, the brittle behavior at shallow levels of the crust is not adequately represented. Specifically, there was no provision for strain localization and formation of brittle faults in these models. Therefore, processes such as the splaying of faults at shallow depths that could lead to disruption and repetition of the coherent IMS in some regions cannot be captured in their model. Microstructures related to shearing, such as mylonites, would also develop at this stage. At least some of the differences in the nature of the IMS in Sikkim, Nepal, and the Kishtwar Window in Zanskar discussed above are likely due to differences in this late stage, shallow level evolutionary history (brittle domain behavior, role of erosion) as well as structural geometry of the regions.

SUMMARY

Using different methods of thermobarometry and consideration of the controls of bulk chemistry, it has been possible to establish that the inverted Barrovian sequence in the lesser Himalaya of Sikkim constitutes a coherent package where both pressure and temperature increase continually as a function of structural height. At the very highest level there may be a slight flattening of the metamorphic field gradient. The misplaced faith on rim compositions of garnets at all grades for carrying out geothermobarometry accounts for much of the controversy associated with the origin of the inverted metamorphism in the Himalaya. Producing a coherent package with an inverted gradient in pressure as well as temperature is not well explained by most models of inverted metamorphism that have been suggested so far. On the other hand, the more recent models of channel flow type tectonics are capable of producing these features. In particular, when the high heat generation of Himalayan pelites is taken into account, such models of subduction followed by collision invariably lead to partial melting of crustal material within plausible (~ 30 million years) timescales. The

sudden drop in density as well as viscosity at depth due to melting triggers uplift and exhumation of the overlying pile. Numerical simulations (Faccenda and others, 2008) using a wide range of parameters relevant to metamorphism in Sikkim show that an inevitable consequence of this process is also the inversion of coherent blocks, and their subsequent exhumation. As high heat generation and partial melting are well documented features of the Himalayan metamorphic pile, melting induced inversion and exhumation of the overlying pile via channel flow type tectonics (Beaumont and others, 2006; Faccenda and others, 2008) is a logical consequence. Subsequently at shallower levels, lower temperature brittle processes of faulting and fold-thrust tectonics must variably modify the geometry of these sequences before final exposure. This process is subject to different geometric and kinematic constraints in different sections of the mountain belt, and most likely leads to the lateral variation in the nature of the exposed inverted sequences along the Himalayan mountain chain.

ACKNOWLEDGMENTS

We acknowledge generous support from the Deutsche Forschungsgemeinschaft (DFG) that enabled this work. DFG grant CH166/8−1 and CH 166/8−3 supported field and analytical work and the stay of SN in Bochum. A Mercator Guest Professorship from the DFG financed the stay of SDG in Bochum. Without the help of several individuals in Bochum this work would not have been possible: Heinz Juergen Bernhard (maintenance and help in the electron microprobe lab), Thomas Fockenberg (XRF and other chemical work), Tanja Westphal and Ellen Kessler (thin section preparation) and Renate Lehmann (drafting). Kathrin Faak and Rauno Baese helped with tables, figures and checking references. Further afield, Deepak Kumar, Subba Kumar, Ganesh Subba, Robin Gurung and Tempa Chophel were enthusiastic participants in the process of observing and then shipping part of the Sikkim Himalaya to Bochum. Back in Bochum, Thomas Murad hauled the rocks all the way from the port in Hamburg and then joined hands with Daniela Luettgebutter to saw numerous rock slabs.

The Council of Scientific and Industrial Research (CSIR) in India supported some of the field work of SDG, he further acknowledges financial support from the J. C. Bose Fellowship. Years of field mapping was carried out by SN as a member of the Geological Survey of India (GSI) team. Numerous interactions with Ralf Dohmen, Fidel Costa and Jiba Ganguly during his stay in Bochum sharpened our concepts of equilibrium and mass transport mediated by fluids. Very constructive criticisms by R. A. Jamieson, D. L. Whitney and J. Ague on an earlier version, and John Ferry on the current version, were the driving force for high grade metamorphism of the manuscript. We thank all of these individuals and organizations for their contributions to this project.

SUPPLEMENTARY DATA TABLES

http://earth.geology.yale.edu/~ajs/SupplementaryData/2008/08DasguptaTable1.pdf
http://earth.geology.yale.edu/~ajs/SupplementaryData/2008/09DasguptaTable2.doc
http://earth.geology.yale.edu/~ajs/SupplementaryData/2008/10DasguptaTable3A.doc
http://earth.geology.yale.edu/~ajs/SupplementaryData/2008/11DasguptaTable3B.doc
http://earth.geology.yale.edu/~ajs/SupplementaryData/2008/12DasguptaTable3C.doc
http://earth.geology.yale.edu/~ajs/SupplementaryData/2008/13DasguptaTable3D.doc
http://earth.geology.yale.edu/~ajs/SupplementaryData/2008/14DasguptaTable3E.doc
http://earth.geology.yale.edu/~ajs/SupplementaryData/2008/15DasguptaTable3F.doc
http://earth.geology.yale.edu/~ajs/SupplementaryData/2008/16DasguptaTable3G.doc

REFERENCES

Ague, J. J., 1991, Evidence for major mass transfer and volume strain during regional metamorphism of pelites: Geology, v. 19, p. 855–858, doi:10.1130/0091-7613(1991)019<0855:EFMMTA>2.3.CO;2.

——— 1994a, Mass transfer during Barrovian metamorphism of pelites, south central Connecticut. I: Evidence for changes in composition and volume: American Journal of Science, v. 294, p. 989–1057.

——— 1994b, Mass transfer during Barrovian metamorphism of pelites, south−central Connecticut. II: Channelized fluid flow and the growth of staurolite and kyanite: American Journal of Science, v. 294, p. 1061–1134.

——— 1997, Crustal mass transfer and index mineral growth in Barrow's garnet zone, northeast Scotland: Geology, v. 25, p. 73–76, doi:10.1130/0091-7613(1997)025<0073:CMTAIM>2.3.CO;2.

Beaumont, C., Nguyen, M. H., Jamieson, R. A., and Lee, B., 2006, Crustal flow modes in large hot orogens, *in* Law, R. D., Searle, M. P., and Godin, L., editors, Channel flow, ductile extrusion, and exhumation in continental collision zones: Geological Society, London, Special Publications, v. 268, p. 91–145, doi: 10.1144/GSL.SP.2006.268.01.05.

Berman, R. G., 1988, Internally-consistent thermodynamic data for stoichiometric minerals in the system Na_2O-K_2O-CaO-MgO-FeO-Fe_2O_3-Al_2O_3-SiO_2-TiO_2-H_2O-CO_2: Journal of Petrology, v. 29, p. 445–522.

——— 1990, Mixing properties of Ca-Mg-Fe-Mn garnets: American Mineralogist, v. 75, p. 328–344.

Beyssac, O., Bollinger, L., Avouac, J. P., and Goffe, B., 2004, Thermal metamorphism in the lesser Himalaya of Nepal determined from Raman spectroscopy of carbonaceous material: Earth and Planetary Science Letters, v. 225, p. 233–241, doi:10.1016/j.epsl.2004.05.023.

Bose, P. M., 1891, Notes on the geological and mineral resources of Sikkim (with primitive maps): Records of the Geological Survey of India, v. 24, 40 p.

Breeding, C. M., and Ague, J. J., 2002, Slab-derived fluids and quartz-vein formation in an accretionary prism, Otago schist, New Zealand: Geology, v. 30, p. 499–502, doi:10.1130/0091-7613(2002)030<0499:SDFAQV>2.0.CO;2.

Brimhall, G. H., Lewis, C. J., Ague, J. J., Dietrich, W. E., Hampel, J., Teague, T., and Rix, P., 1988, Metal enrichment in bauxites by deposition of chemically mature aeolian dust: Nature, v. 333, p. 819–824, doi:10.1038/333819a0.

Burnham, C. W., Holloway, J. R., and Davis, N. F., 1969, Thermodynamic properties of water to 1000°C and 10,000 bars: Geological Society of America Special Paper, v. 132, 96 p.

Catlos, E. J., Harrison, T. M., Kohn, M. J., Grove, M., Ryerson, F. J., Manning, C. E., and Upreti, B. N., 2001, Geochronologic and thermobarometric constraints on the evolution of the Main Central Thrust, central Nepal, Himalaya: Journal of Geophysical Research, v. 106, p. 16,177–16,204, doi:10.1029/2000JB900375.

Catlos, E. J., Dubey, C. S., Harrison, T. M., and Edwards, M. A., 2004, Late Miocene movement within the Himalayan Main Central Thrust shear zone, Sikkim, north-east India: Journal of Metamorphic Geology, v. 22, p. 207–226, doi:10.1111/j.1525-1314.2004.00509.x.

Chakraborty, S., and Ganguly, J., 1991, Compositional zoning and cation diffusion in aluminosilicate garnets, *in* Ganguly, J., editor, Diffusion, Atomic Ordering and Mass Transfer: Berlin, Heidelberg, New York, Toronto, Springer-Verlag, Advances in Physical Geochemistry, v. 8, p. 120–175.

Chakraborty, S., Dasgupta, S., and Neogi, S., 2003, Generation of migmatites and the nature of partial melting in a continental collision zone setting: An example from the Sikkim Himalaya: Indian Journal of Geology, v. 75, p. 38–53.

——— 2007, Nucleation kinetics controlled by chemical overstepping and its tectonic implications: An example from the Sikkim Himalaya: European Journal of Mineralogy, v. 19, p. 791–803, doi:10.1127/0935-1221/2007/0019-1775.

Chamberlain, C. P., Zeitler, P. K., and Erickson, E., 1991, Constraints on the tectonic evolution of the northwest Himalaya from geochronologic and petrologic studies of Babusar Pass, Pakistan: Journal of Geology, v. 99, p. 829–849.

Chatterjee, N. D., 1972, The upper stability limit of the assemblage paragonite + quartz and its natural occurrences: Contributions to Mineralogy and Petrology, v. 34, p. 288–303, doi:10.1007/BF00373759.

Daniel, C. G., Hollister, L. S., Parrish, R. R., and Grujic, D., 2003, Exhumation of the Main Central Thrust from lower crustal depths, eastern Bhutan Himalaya: Journal of Metamorphic Geology, v. 21, p. 317–334, doi: 10.1046/j.1525-1314.2003.00445.x.

Dasgupta, S., Ganguly, J., and Neogi, S., 2004, Inverted metamorphic sequence in the Sikkim Himalayas: Crystallization history, P-T gradient, and implications: Journal of Metamorphic Geology, v. 22, p. 395–412, doi:10.1111/j.1525-1314.2004.00522.x.

Davidson, C., Grujik, D. E., Hollister, L. S., and Schmid, S. M., 1997, Metamorphic reactions related to decompression and synkinematic intrusion of leucogranite, High Himalayan Crystallines, Bhutan: Journal of Metamorphic Geology, v. 15, p. 593–612, doi:10.1111/j.1525-1314.1997.00044.x.

Droop, G. T. R., and Harte, B., 1995, The effect of Mn on the phase relations of medium−grade pelites: Constraints from natural assemblages on petrogenetic grid topology: Journal of Petrology, v. 36, p. 1549–1578.

Dubey, C. S., Catlos, E. J., and Sharma, B. K., 2005, Modelling of P-T-t paths constrained by mineral chemistry and monazite dating of metapelites in relationship to MCT activity in Sikkim Eastern Himalayas, *in* Thomas, H., editor, Metamorphism and Crustal Evolution: New Delhi, Atlantic Publishers, p. 250–282.

Faccenda, M., Gerya, T. V., and Chakraborty, S., 2006, Styles of incipient orogeny: insight from numerical modeling and observation: AGU, EOS Transactions, 87(52), Fall Meeting Supplement, Abstract T13C-0523.

Faccenda, M., Gerya, T. V., and Chakraborty, S., 2008, Styles of post-subduction collisional orogeny: influence of convergence velocity, crustal rheology and radiogenic heat production: Lithos, v, 103, p. 257–287, doi:10.1016/j.lithos.2007.09.009.

Fraser, G., Worley, B., and Sandiford, M., 2000, High precision geothermobarometry across the High Himalayan metamorphic sequence, Langtang valley, Nepal: Journal of Metamorphic Geology, v. 18, p. 665–681, doi:10.1046/j.1525-1314.2000.00283.x.

Ganguly, J., and Saxena, S. K., 1987, Mixtures and mineral reactions: Berlin, Springer-Verlag, 291 p.

Ganguly, J., Cheng, W., and Tirone, M., 1996, Thermodynamics of aluminosilicate garnet solid solution: new experimental data, an optimized model and thermometric applications: Contributions to Mineralogy and Petrology, v. 126, p. 137–151, doi:10.1007/s004100050240.

Ganguly, J., Dasgupta, S., Cheng, W., and Neogi, S., 2000, Exhumation history of a section of the Sikkim Himalayas, India: records in the metamorphic mineral equilibria and compositional zoning of garnet: Earth and Planetary Science Letters, v. 183, p. 471–486, doi:10.1016/S0012-821X(00)00280-6.

Grujic, D., Casey, M., Davidson, C., Hollister, L. S., Kundig, R., Pavlis, T., and Schmid, S., 1996, Ductile extrusion of the High Himalayan Crystalline in Bhutan: evidence from quartz microfabrics: Tectonophysics, v. 260, p. 21–43, doi:10.1016/0040-1951(96)00074-1.

Guillot, S., 1999, An overview of the metamorphic evolution in Central Nepal: Journal of Asian Earth Sciences, v. 17, p. 713–725, doi:10.1016/S1367-9120(99)00045-0.

Harris, N. B. W., Caddick, M., Kosler, J., Goswami, S., Vance, D., and Tindle, A. G., 2004, The pressure-temperature-time path of migmatites from the Sikkim Himalaya: Journal of Metamorphic Geology, v. 22, p. 249–264, doi:10.1111/j.1525-1314.2004.00511.x.

Hodges, K. V., 2000, Tectonics of the Himalaya and southern Tibet from two perspectives: Geological Society of America Bulletin, v. 112, p. 324–350, doi:10.1130/0016-7606(2000)112<0324:TOTHAS>2.3.CO;2.

Hodges, K. V., and Silverberg, D. S., 1988, Thermal evolution of the greater Himalaya, Garhwal, India: Tectonics, v. 7, p. 583–600, doi:10.1029/TC007i003p00583.

Hodges, K. V., Burchfiel, B. C., Royden, L. H., Chen, Z., and Liu, Y., 1993, The metamorphic signature of contemporaneous extension and shortening in the central Himalayan orogen: data from the Nyalam transect, southern Tibet: Journal of Metamorphic Geology, v. 11, p. 721–737, doi:10.1111/j.1525-1314.1993.tb00183.x.

Hoisch, T. D., 1990, Empirical calibration of six geobarometers for the mineral assemblage quartz+muscovite+biotite+plagioclase+garnet: Contributions to Mineralogy and Petrology, v. 104, p. 225–234, doi:10.1007/BF00306445.

Holdaway, M. J., 2000, Application of new experimental and garnet Margules data to the garnet-biotite geothermometer: American Mineralogist, v. 85, p. 881–892.

Holdaway, M. J., Dutrow, B. L., and Hinton, R. W., 1988, Devonian and carboniferous metamorphism in west-central Maine: the muscovite-almandine geobarometer and the staurolite problem revisited: American Mineralogist, v. 73, p. 20–47.

Holland, T. J. B., and Powell, R., 1998, An internally consistent thermodynamic dataset for phases of petrological interest: Journal of Metamorphic Geology, v. 16, p. 309–343, doi:10.1111/j.1525-1314.1998.00140.x.

Hubbard, M. S., 1996, Ductile shear as a cause of inverted metamorphism: example from the Nepal Himalaya: Journal of Geology, v. 104, p. 493–499.

——— 1989, Thermobarometric constraints on the thermal history of the Main Central thrust zone and Tibetan Slab, eastern Nepal Himalaya: Journal of Metamorphic Geology, v. 7, p. 19–30, doi:10.1111/j.1525-1314.1989.tb00572.x.

Inger, S., and Harris, N. B. W., 1992, Tectonothermal evolution of the High Himalayan Crystalline Sequence, Langtang Valley, northern Nepal: Journal of Metamorphic Geology, v. 10, p. 439–452, doi:10.1111/j.1525-1314.1992.tb00095.x.

Jain, A. K., and Manickavasagm, R. M., 1993, Inverted metamorphism in the intracontinental ductile shear zone during Himalayan collision tectonics: Geology, v. 21, p. 407–410, doi:10.1130/0091-7613(1993)021<0407:IMITID>2.3.CO;2.

Jain, A. K., Singh. S., and Manickavasagam, R. M., 2002, Himalayan Collision Tectonics: Gondwana Research Group Memoir, No. 7, 114 p.

Jamieson, R. A., Beaumont, C., Fullsack, P., and Lee, B., 1998, Barrovian regional metamorphism: Where's the heat?, *in* Treloar, P. J., and O'Brien, P. J., editors, What Drives Metamorphism and Metamorphic Reactions?: Geological Society, London, Special Publications, v. 138, p. 23–51, doi: 10.1144/GSL.SP.1996.138.01.03.

Jamieson, R. A., Beaumont, C., Nguyen, M. H., and Grujic, D., 2006, Provenance of the Greater Himalayan Sequence and associated rocks: Predictions of channel flow models, *in* Law, R. D., Searle, M. P., and Godin, L., editors, Channel flow, Ductile Extrusion and Exhumation in Continental Collision Zones: Geological Society, London, Special Publications, v. 268, p. 165–182, doi: 10.1144/GSL.SP.2006.268.01.07.

Johnson, M. R. W., and Harley, S. H., 2003, Comment on "Kinematic model for the Main Central Thrust in Nepal": Geology, Online Forum p. e40, doi: 10.1130/0091-7613(2003)31<e40:KMFTMC>2.0.CO;2.

Kohn, M. J., Catlos, E. J., Ryerson, F. J., and Harrison, T. M., 2001, Pressure-temperature–time path discontinuity in the Main Central thrust zone, central Nepal: Geology, v. 29, p. 571–574, doi: 10.1130/0091-7613(2001)029<0571:PTTPDI>2.0.CO;2.

Macfarlane, A. M., 1995, An evaluation of the inverted metamorphic gradient at Langtang National Park, central Nepal Himalaya: Journal of Metamorphic Geology, v. 13, p. 595–612, doi:10.1111/j.1525-1314.1995.tb00245.x.

Macfarlane, A., Sorkhabi, R. B., and Quade, J., 1999, Himalaya and Tibet: Mountain Roots to Mountain Tops: Geological Society of America Special Paper 328, 330 p.

Mahar, E. M., Baker, J. M., Powell, R., Holland, T. J. B., and Howell, N., 1997, The effect of Mn on mineral stability in metapelites: Journal of Metamorphic Geology, v. 15, p. 223–238, doi:10.1111/j.1525-1314.1997.00011.x.

Mallet, F. R., 1874, On the geology and mineral resources of the Darjeeling district and western Duars: Memoirs of the Geological Survey of India, v. 11, p. 1–50.

Mohan, A., Windley, B. F., and Searle, M. P., 1989, Geothermobarometry and development of Inverted Metamorphism in the Darjeeling–Sikkim region of the Eastern Himalaya: Journal of Metamorphic Geology, v. 7, p. 95–110, doi:10.1111/j.1525-1314.1989.tb00577.x

Moss, B. E., Haskin, L. A., and Dymek, R. F., 1996, Compositional variations in metamorphosed sediments of the Littleton Formation, New Hampshire, and the Carrabassett Formation, Maine, at sub-hand specimen, outcrop, and regional scales: American Journal of Science, v. 296, p. 473–505.

Mukhopadhyay, B., Holdaway, M. J., and Koziol, A. M., 1997, A statistical model of thermodynamic mixing properties of Ca-Mg-Fe_2+ garnets: American Mineralogist, v. 82, p. 165–181.

Neogi, S., ms, 1993, Petrotectonics of the Central Crystalline Complex of Sikkim and its implication in the evolution of the Himalayas: Kolkata, Jadavpur University, Ph.D. Thesis, 132 p.

Neogi, S., Dasgupta, S., and Fukuoka, M., 1998, High *P-T* polymetamorphism, dehydration-melting, and generation of migmatites and granites in the Higher Himalayan crystalline complex, Sikkim, India: Journal of Petrology, v. 39, p. 61–99, doi:10.1093/petrology/39.1.61.

Pecher, A., 1989, The metamorphism in the central Himalaya: Journal of Metamorphic Geology, v. 7, p. 31–41, doi:10.1111/j.1525-1314.1989.tb00573.x.

Powell, R., and Holland, T. J. B., 1988, An internally consistent dataset with uncertainties and correlations; 3, Applications to geobarometry, worked examples and a computer program: Journal of Metamorphic Geology, v. 6, p. 173–204, doi:10.1111/j.1525-1314.1988.tb00415.x.

Ray, C., 1949, Regional metamorphism in eastern Sikkim: Quarterly Journal of the Geological, Mining and Metallurgical Society of India, v. 21, p. 155–170.

Ray, S., 1947, Zonal metamophism in Eastern Himalaya and some aspects of local Geology: Quarterly Journal of the Geological, Mining and Metallurgical Society of India, v. 19, p. 117–140.

Robinson, D. M., De Celles, P. G., Garzione, C. N., Pearson, O. N., Harrison, T. M., and Catlos, E. J., 2003, Kinematic model for the Main Central Thrust in Nepal: Geology, v. 31, p. 359–362, doi:10.1130/0091-7613(2003)031<0359:KMFTMC>2.0.CO;2.

Searle, M. P., and Szulc, A. G., 2005, Channel flow and ductile extrusion of the high Himalayan slab-the Kangchenjunga–Darjeeling profile, Sikkim Himalaya: Journal of Asian Earth Sciences, v. 25, p. 173–185, doi:10.1016/j.jseaes.2004.03.004.

Sinha-Roy, S., 1982, Himalayan Main Central Thrust and its implications for Himalayan inverted metamorphism: Tectonophysics, v. 84, p. 197–224, doi:10.1016/0040-1951(82)90160-3.

Spear, F. S., Kohn, M. J., and Paetzold, S., 1995, Petrology of the regional sillimanite zone, west-central New Hampshire, U.S.A., with implications for the development of inverted isograds: American Mineralogist, v. 80, p. 361–376.

Spear, F. S., Kohn, M. J., and Cheney, J. T., 1999, *P-T* paths from anatectic pelites: Contributions to Mineralogy and Petrology, v. 134, p. 17–32, doi:10.1007/s004100050466.

Stephenson, B. J., Waters, D. J., and Searle, M. P., 2000, Inverted metamorphism and the Main Central Thrust: field relations and thermobarometric constraints from the Kishtwar Window, NW Indian Himalaya: Journal of Metamorphic Geology, v. 18, p. 571–590, doi:10.1046/j.1525-1314.2000.00277.x.

Teyssier, C., and Whitney, D. L., 2002, Gneiss domes and Orogeny: Geology, v. 30, p. 1139–1142, doi:10.1130/0091-7613(2002)030<1139:GDAO>2.0.CO;2.

Tinkham, D. K., Zuluaga, C. A., and Stowell, H. H., 2001, Metapelite phase equilibria modeling in MnNCKFMASH: The effect of variable Al2O3 and MgO/(MgO+FeO) on mineral stability: Geological Material Research, v. 3, p. 1–42.

Treloar, P. J., Williams, M. P., and Coward, M. P., 1989, Metamorphism and crustal stacking in the North Indian Plate, North Pakistan: Tectonophysics, v. 165, p. 167–184, doi:10.1016/0040-1951(89)90045-0.

Vannay, J. C., and Grasemann, B., 1998, Inverted metamorphism in the High Himalaya of Himachal Pradesh (NW India): Phase equilibria versus thermobarometry: Schweizerische Mineralogische und Petrographische Mitteilungen, v. 78, p. 107–132.

Vannay, J-C., and Hodges, K. V., 1996, Tectonometamorphic evolution of the metamorphic core between the Annapurna and Dhaulagiri, central Nepal: Journal of Metamorphic Geology, v. 14, p. 635–656, doi:10.1046/j.1525-1314.1996.00426.x.

Vannay, J. C., Sharp, Z. D., and Grasemann, B., 1999, Himalayan inverted metamorphism constrained by oxygen isotope thermometry: Contributions to Mineralogy and Petrology, v. 137, p. 90–101, doi:10.1007/s004100050584.

Vernon, R. H., 1979, Formation of late sillimanite by hydrogen metasomatism (base-leaching) in some high-grade gneisses: Lithos, v. 12, p. 143–152, doi:10.1016/0024-4937(79)90045-8.

Wang, P., and Spear, F. S., 1991, A field and theoretical analysis of garnet + chlorite + chloritoid + biotite assemblages from the Tri-State (MA, CT and NY) area, USA: Contributions to Mineralogy and Petrology, v. 106, p. 217–235, doi:10.1007/BF00306435.

Wei, C. J., Powell, R., and Clarke, G. L., 2004, Calculated phase equilibria for low- and medium pressure metapelites in KFMASH and KMnFMASH systems: Journal of Metamorphic Geology, v. 22, p. 495–508, doi:10.1111/j.1525-1314.2004.00530.x.